

Abstract

31
32

33 The retrieval of indicators of vegetation stress from remote sensing imagery is an important
34 issue for the accurate assessment of forest decline. The *Photochemical Reflectance Index*
35 (PRI) has been demonstrated as a physiological index sensitive to the epoxidation state of
36 the xanthophyll cycle pigments and to photosynthetic efficiency, serving as a proxy for
37 short-term changes in photosynthetic activity, stress condition, and pigment absorption, but
38 highly affected by illumination conditions, viewing geometry and canopy structure. In this
39 study, a diurnal airborne campaign was conducted over *Pinus sylvestris* and *Pinus nigra*
40 forest areas with the *Airborne Hyperspectral Scanner* (AHS) to evaluate the effects of
41 canopy structure on PRI when used as an indicator of stress in a conifer forest. The AHS
42 airborne sensor was flown at two times (8:00 GMT and 12:00 GMT) over forest areas
43 under varying field-measured stress levels, acquiring 2 m spatial resolution imagery in 80
44 spectral bands in the 0.43-12.5 μm spectral range. Five formulations of PRI (based on R_{531}
45 as a xanthophyll-sensitive spectral band) were calculated using different reference
46 wavelengths, such as PRI_{570} (reference band $R_{\text{REF}}=R_{570}$), and the PRI modifications PRI_{m1}
47 ($R_{\text{REF}}=R_{512}$), PRI_{m2} ($R_{\text{REF}}=R_{600}$), PRI_{m3} ($R_{\text{REF}}=R_{670}$), and PRI_{m4} ($R_{\text{REF}}=R_{570}, R_{670}$), along
48 with other structural indices such as NDVI, SR, OSAVI, MSAVI and MTVI2. In addition,
49 thermal bands were used for the retrieval of the land surface temperature. A radiative
50 transfer modeling method was conducted using the LIBERTY and INFORM models to
51 assess the structural effects on the PRI formulations proposed, studying the sensitivity of
52 PRI_m indices to detect stress levels while minimizing the effects caused by the conifer
53 architecture. The PRI indices were related to stomatal conductance, xanthophyll
54 epoxidation state (EPS) and crown temperature. The modeling analysis showed that the

55 coefficient of variation (CV) for PRI was 50%, whereas the CV for PRI_{m1} (band R₅₁₂ as a
56 reference) was only 20%. Simulation and experimental results demonstrated that PRI_{m1}
57 ($R_{REF}=R_{512}$) was less sensitive than PRI ($R_{REF}=R_{570}$) to changes in Leaf Area Index (LAI)
58 and tree densities. PRI₅₁₂ was demonstrated to be sensitive to EPS at both leaf ($r^2=0.59$) and
59 canopy level ($r^2=0.40$), yielding superior performance than PRI₅₇₀ ($r^2=0.21$) at the canopy
60 level. In addition, PRI₅₁₂ was significantly related to water stress indicators such as
61 stomatal conductance (Gs; $r^2=0.45$) and water potential (Ψ ; $r^2=0.48$), yielding better results
62 than PRI₅₇₀ (Gs, $r^2=0.21$; Ψ , $r^2=0.21$) due to the structural effects found on the PRI₅₇₀ index
63 at the canopy level.

64

65

66

67 **Keywords:** forest decline, water stress, photosynthetic pigments, Airborne Hyperspectral
68 Scanner, photochemical-related indices
69

70

71 **1. Introduction**

72 The Photochemical Reflectance Index (PRI) is a physiological reflectance index sensitive
73 to the epoxidation state of the xanthophyll cycle pigments and to photosynthetic efficiency
74 (Gamon *et al.*, 1992). PRI was proposed by Gamon *et al.* (1992) as a normalized difference
75 of 530 nm and a reference band at 550 nm, related to photosynthetic processes and affected
76 by xanthophyll pigment absorption. Several studies report good results using 550 (or 551)
77 nm as a reference wavelength (Peñuelas *et al.*, 1994 and Middleton *et al.*, 2009). Based on
78 research on leaves exposed to short-term changes in illumination, several studies (Peñuelas
79 *et al.*, 1995; Gamon *et al.*, 1993; and Gamon *et al.*, 1997) found that 570 nm appeared to be
80 a better reference wavelength. Since then, PRI has been applied by using 570 nm as a
81 standard reference at leaf and canopy levels (Sims and Gamon, 2002; Suárez *et al.*, 2010).
82 For example, the accumulation of de-epoxidated (DEPS) forms of xanthophyll cycle
83 pigments was found by Peguero-Pina and co-workers in a silver fir stand growing under
84 Mn deficiency (Peguero-Pina *et al.*, 2007) and *Quercus coccifera* growing under intense
85 drought (Peguero-Pina *et al.*, 2008), assessing the stress effects on leaf PRI. Later, Filella *et*
86 *al.* (2009) found significant correlation between PRI and DEPS across seasons and
87 treatments for *Pinus sylvestris* and *Quercus ilex*. PRI was also related to
88 carotenoid/chlorophyll ratio and b-carotene/chlorophyll ratio. It was only under brief
89 variations in illumination conditions that PRI was correlated with DEPS, but was not
90 related to other leaf pigments such as other carotenoids (Car) and chlorophyll a+b (Cab).
91 Recent work (Suárez *et al.*, 2009) demonstrated that PRI is a *pre-visual* water stress
92 indicator in crops, but suggested that radiative transfer models were required to account for
93 Cab and LAI effects for estimating the theoretical canopy PRI to help separating between
94 stress levels. Nevertheless, such work relied on results obtained from tree crowns when

95 targeting pure vegetation, thus causing smaller structural effects on PRI than forest canopy
96 architectures. In addition, assessing plant physiological condition based on PRI at canopy
97 scale is a difficult approach due to the different factors affecting this index, such as viewing
98 and illumination geometry effects, crown architecture and shadow/sunlit fraction (Barton
99 and North, 2001; Hall *et al.*, 2008; Hilker *et al.*, 2008; Middleton *et al.*, 2009; Suárez *et al.*,
100 2008).

101

102 At the leaf level, additional PRI formulations have been proposed using varying reference
103 wavelengths (Filella *et al.*, 1996; Gamon *et al.*, 1992; Inoue *et al.*, 2008; Peñuelas *et al.*,
104 1994). Many studies adopted 570 nm, largely based on the observation that it provided a
105 good reference wavelength for leaf-level studies (Gamon *et al.*, 1993; Peñuelas *et al.*, 1995;
106 Gamon *et al.*, 1997). At canopy scale, Gamon *et al.* (1992) showed how reflectance at
107 several wavebands (from 539 to 670 nm) in combination with 531 nm worked rather well,
108 and that 550 nm was the best overall reference wavelength based on a combination of
109 statistical tests (regression, principle components analysis). This wavelength seemed to
110 best correct for "greenness" (i.e., canopy structure) effects. Other studies showed similar
111 good results with 551 nm as a reference (the nearest MODIS band) (Middleton *et al.*,
112 2009). Most authors adopted 570 nm as a reference, although the sensitivity of this index to
113 structural and illumination effects were demonstrated (Suárez *et al.*, 2008).

114

115 Forest decline is expressed through multiple effects due to an array of interacting biotic and
116 abiotic factors. Assessing stress condition of a forest in decline using PRI is a complex
117 problem because of the different alterations of the tree at the canopy- and stand-level (e.g.,
118 changes in Leaf Area Index (LAI), Fraction of Photosynthetically Active Radiation (FPAR)

119 and Leaf Angle Distribution (LAD), vegetation cover or stand density); at the leaf level,
120 with alterations in photosynthetic activity, pigment content, and internal leaf structure; and
121 at the cell level, with changes in water content, among others (Melzack *et al.*, 1985). In the
122 past, conifer forests in decline were assessed by changes in vegetation indices related to
123 canopy structure, such as LAI (Schlerf *et al.*, 2005; Schlerf and Atzberger, 2006), and
124 chlorophyll concentration (Zarco-Tejada *et al.*, 2004; Moorthy *et al.*, 2008; Zhang *et al.*,
125 2008). However, when canopy chlorophyll concentration or total leaf area is affected by
126 water stress, damage to the plant has already occurred, and plant status is compromised.
127 The detection of stress in its early phase is normally defined as pre-visual and takes place
128 before there are structural (visual) effects or consequences of the stress; this is critical
129 information required for the assessment of forest decline. These processes related to water
130 stress have affected important areas in Spain and other European countries (Allen *et al.*,
131 2010; Martínez-Vilalta *et al.*, 2008; Navarro-Cerrillo *et al.*, 2007; Rebetez and Dobbertin,
132 2004). Such studies demonstrate that drought plays an important role in Mediterranean
133 forest decline, especially in species sensitive to water stress like *Pinus sylvestris* (Martínez-
134 Vilalta *et al.*, 2008; Poyatos *et al.*, 2008). Research has shown that in an early stage of
135 stress, before damage has occurred, photosynthesis declines. Under these conditions, the
136 absorbed light exceeds the photosynthetic demand, and plants react with mechanisms for
137 dissipating this excess energy non-destructively (Björkman and Demmig-Adams, 1994).
138 One mechanism is linked to xanthophyll cycle activation, where pigment violaxanthin is
139 converted into antheraxanthin and zeaxanthin via de-epoxidase reactions (Yamamoto,
140 1979). Several manuscripts have revealed a close relationship between xanthophyll
141 pigment conversions and excess energy dissipation in the leaf pigments associated with
142 photosystem II (PSII) (Demmig-Adams and Adams, 1996). Another stress indicator

143 suggested in several studies (proposed by Jackson *et al.*, 1977) is the temperature of the
144 canopy as an indicator of tree transpiration. Thermal remote sensing of water stress has
145 been successfully applied to tree crop canopies based on high resolution thermal remote
146 sensing imagery (Berni *et al.*, 2009), airborne thermal imagery (Sepulcre-Cantó *et al.*,
147 2007) and satellite thermal information in combination with 3D radiative transfer models to
148 understand the effects of scene thermal components on large ASTER pixels (Sepulcre-
149 Cantó *et al.*, 2009).

150

151 However, very few references have shown feasible remote sensing methods for
152 successfully linking remote sensing indices and physiological variables by focusing on the
153 *pre-visual* detection of forest decline before damage is visible. At canopy scale, most of this
154 research has dealt primarily with photosynthetic light use efficiency and carbon dioxide
155 using satellite images such as the Moderate Resolution Imaging Spectroradiometer data
156 (MODIS) (Drolet *et al.*, 2005; Garbulsky *et al.*, 2008; Hilker *et al.*, 2009) or EO-1
157 Hyperion data (Asner *et al.*, 2005). Nevertheless, few of these studies are focused on PRI
158 and other spectral indices validated with *in situ* measurements of EPS in heterogeneous
159 forest ecosystems. Questions need to be answered regarding PRI interpretation on forest
160 canopies where crown mixture, shadows and tree architecture play a critical role in
161 physiological remote sensing indices. The present study provides new insights into the
162 understanding of PRI as an indicator of stress on complex canopies, analyzing the effects
163 on PRI formulations due to the structure. The study assesses imaged PRI and model-
164 simulated PRI obtained through radiative transfer simulation of conifer canopies,
165 evaluating the sensitivity of PRI formulations to EPS while minimizing canopy structural
166 effects.

167

168 **2. Material and Methods**

169 **2.1. Study area selection**

170 The experimental area is located in Sierra de Filabres (Almeria province, southeastern
171 Spain) (37° 13' 27" N, 2° 32' 54" W) (Figure 1), the driest region in Western Europe. The
172 elevation of the study area ranges from 1540 to 2000 m.a.s.l., and annual rainfall is between
173 300 and 400 mm. The annual average temperature is 11°C, reaching a maximum of 32°C
174 during summer and a minimum of -8°C during winter. The vegetation consists of a 40-year-
175 old mixed pine afforestation of *Pinus nigra* Arnold and *Pinus sylvestris* L. (Table 1 and 2).
176 Within the forest stands, sparse evergreen shrub vegetation (*Adenocarpus decorticans*
177 Boiss. and *Cistus laurifolius* L.) partially covers the ground. Parent material is composed of
178 siliceous rock with quartz micaschists, forming eutric cambisol-regosol soils.

179

180

181 **2.2. Field data collection**

182 Field sampling campaigns were conducted concurrently with airborne overflights during
183 the last week of July 2008. Two sets of measurements were collected at 8:00 and 12:00
184 (GMT). The monitored trees consisted of 36 *Pinus nigra* and 36 *Pinus sylvestris*, located in
185 three study areas (12 trees per study areas). Table 3 shows the mean values and the standard
186 deviation of xanthophyll epoxidation state (EPS), water potential (ψ) and stomatal
187 conductance (Gs) calculated for each study area at 12:00 GMT. To test the null hypothesis
188 that EPS, water potential, and stomatal conductance were not significantly different among
189 study areas, a one-way ANOVA analysis was conducted using a significance level of 0.05.
190 A Tukey's post-hoc analysis was performed to evaluate differences between study areas. In

191 the case of water potential a Kruskal-Wallis (KW) test was applied because the data were
192 not normally distributed. The variables measured showed significant differences in the
193 physiological status for each study area ($p < 0.05$).

194 The measurements were conducted on trees of similar height (Table 2) located in low slope
195 areas ($< 10\%$), therefore with a similar sun/shade fraction. The trees are largely the same
196 age since they were part of a reforestation program undertaken by the Spanish government
197 in 1980.

198

199 Physiological parameters measured from the selected trees were total concentration of
200 chlorophyll (chlorophyll a (chl_a) and chlorophyll b (chl_b)), needle water content and dry
201 mass, stomatal conductance (using a portable gas exchange system CIRAS-1 instrument,
202 PP Systems, Hitchin Herts, UK) and crown temperature (using an infrared thermometer,
203 Optris LS, DE). These data were averaged from four measurements per tree during each
204 period at the time of the AHS imagery acquisition (8:00 and 12:00, GMT). Field Gas
205 exchange measurements were performed in attached leaves at controlled CO_2 external
206 concentration ($C_a = 350$ ppm) and ambient relative humidity. Stomatal conductance (G_s)
207 was estimated using gas exchange data and the total needle area exposed obtained from
208 photos taken for each measurement. Predawn (Ψ_{pd} , 4:00 GTM) and midday (Ψ_m , 12:00
209 GTM) xylem water potential (pressure chamber, SKPM 1400, Skye Instruments, UK)
210 (Scholander *et al.*, 1965) were also measured. LAI was estimated with a PCA (Plant
211 Canopy Analyzer, LAI-2000, LI-COR, Lincoln, NE, USA).

212

213 **2.3. Leaf-level measurements**

214 Leaf-level measurements were collected on a total of 15 needles per tree, five needles per
215 needle age (current-year, n; young, n+1; and mature, n+3), with a total of 540 needles
216 measured per species. The needles were collected from the top of the crown by selecting
217 branches of illuminated areas. Two sets of needles were collected from the same shoots at
218 the time of the AHS flights, 8:00 and 12:00 (GMT). One set was placed under cold storage
219 in coolers, and the other set was frozen in liquid nitrogen in the field. Both storage
220 conditions were in darkness, and the needles were harvested and immediately frozen in the
221 field. The first set was transported directly to the laboratory and used to measure leaf
222 spectral reflectance and transmittance, and water content. The second set was kept under
223 -80°C and used for pigment analysis by destructive methods.

224

225 Needle pigments were extracted as reported by Abadía and Abadía (1993). Pigment extracts
226 were obtained from a mixed sample of 5 cm of needle material, 1 linear cm per needle. The
227 area was calculated by assuming the needle to be a half cylinder and the diameter to be the
228 measured width of each needle. Needle diameter was measured with a digital caliper
229 precision instrument. Pigment content was obtained based on this area. Five consecutive
230 centimeters were also cut for structural measurements (thickness and width), water content
231 and dry mass. The needles were ground in a mortar on ice with liquid nitrogen and diluted
232 in acetone up to 5 ml (in the presence of Na ascorbate). Then, the extracts were filtered
233 through a 0.45- μ m filter to separate the pigment extracts from the Na ascorbate. The
234 spectrophotometric and High-Performance Liquid Chromatography (HPLC) determinations
235 were carried out simultaneously on the same extracts, 20 μ l were injected into the HPLC
236 and 1 ml was inserted into the spectrophotometer. The extractions and measurements were
237 undertaken concurrently to avoid pigment degradation. Absorption at 470, 644.8 and 661.6

238 nm was measured with the spectrophotometer to derive chlorophyll *a* and *b*, and total
239 carotenoid concentrations (Abadía and Abadía, 1993) and pigment extracts were analyzed
240 using an isocratic HPLC method (Larbi *et al.*, 2004). Samples were injected into a 100×8
241 mm Waters Novapak C18 radial compression column (4 μm particle size) with a 20 μl loop,
242 and mobile phases were pumped by a Waters M45 high pressure pump at a flow of 1.7
243 ml/min. The EPS ratio between the pigment concentration was calculated as
244 $(V+0.5A)/(V+A+Z)$ (Thayer & Björkman, 1990), where V is violaxanthin, A is
245 antheraxanthin and Z is zeaxanthin.

246 Optical measurements were taken on needles from a total of 42 trees, 21 trees per species.
247 Needle reflectance and transmittance were measured with a Li-Cor 1800-12 integrating
248 sphere (Li-Cor, Lincoln, NE, USA) coupled to a fiber optic spectrometer (Ocean Optics
249 model USB2000 spectrometer, Ocean Optics, Dunedin, FL, USA), using the method
250 described in Moorthy *et al.* (2008) and Zarco-Tejada *et al.* (2004). Needle reflectance and
251 transmittance measurements of *Pinus nigra* (Figures 2a and b) and *Pinus sylvestris* (Figures
252 2c and d) showed variations in the visible spectral region due to stress levels affecting both
253 chlorophyll and xanthophyll pigments. Needle spectral reflectance was also measured with
254 a UniSpec Spectral Analysis System (PP Systems, Herts, UK), following a similar
255 procedure to that described by Richardson and Berlyn (2002). The Unispec measurements
256 were conducted in the field minutes before the needles were collected.

257

258 **2.4. Airborne image acquisitions**

259 The airborne campaign was conducted by the Spanish Aerospace Institute (INTA) with the
260 Airborne Hyperspectral Scanner AHS (Sensytech Inc., currently Argon St. Inc., Ann Arbor,
261 MI, USA) during the last week of July 2008. The airborne data acquisition was carried out

262 at 8:00 GMT and 12:00 GMT, acquiring 2 m spatial resolution imagery in 38 bands in the
263 0.43-12.5 μm spectral range. The Field of View (FOV) and Instantaneous Field of View
264 (IFOV) of the AHS sensor were 90° and 2.5 mrad respectively, and plots were located in
265 the central region of the scene in order to avoid edge effects. *At-sensor* radiance processing
266 and atmospheric correction were performed at the INTA facilities. Atmospheric correction
267 was conducted with ATCOR4 based on the MODTRAN radiative transfer model (Berk *et*
268 *al.*, 1998; 2000) using aerosol optical depth at 550 nm collected with a Micro-Tops II sun
269 photometer (Solar Light, Philadelphia, PA, USA). Land surface temperature retrieval from
270 thermal remote sensing data was obtained with the two-channel algorithm proposed by
271 Sobrino *et al.* (2002; 2006), taking into account emissivity and water vapor effects. The
272 emissivity value applied for vegetation was 0.98. A full description of land surface
273 temperature retrieval from thermal imagery via AHS can be found in Sepulcre-Cantó *et al.*
274 (2006) and Sobrino *et al.* (2006) . The mean air temperature during the flight was 20.9°C
275 (± 0.05) at 8:00 GMT and 24.5°C (± 0.11) at 12:00 GMT. The temperature data were
276 collected by the meteorological station at Calar Alto Astronomical Observatory, located
277 within the study area.

278 Vegetation indices were calculated to track changes in canopy structure and pigment
279 concentration as a function of the stress condition. The AHS spectra (Figure 1c) were
280 extracted from the imagery at windows of 3x3 pixels. Pure vegetation pixels were located
281 by selecting the pixels with NDVI higher than 0.6 on 3x3 windows. Figure 3 shows one
282 region of interest extracted for affected and non-affected areas of *Pinus nigra* and *Pinus*
283 *sylvestris*. The airborne reflectance extracted for each tree, and comparing the spectra for
284 stressed and non-stressed study areas (SS1 and SS3) of pure crowns and mixed pixels are
285 shown in Figure 3a and 3b, respectively.

286

287 Spectra extracted from the imagery were related to the field data using pure vegetation
288 pixels (NDVI higher than 0.6). The analysis aimed at assessing the relationships between
289 EPS, G and Ψ and the different PRI formulations calculated to minimize the structural
290 effects on PRI. The index PRI was reformulated as derived from R_{531} (adapted to AHS
291 using band R_{540} as in Suárez *et al.*, 2008) using reference bands R_{512} (PRI_{m1}), R_{600} (PRI_{m2}),
292 R_{670} (PRI_{m3}), and R_{670} and R_{570} (PRI_{m4}) (Table 4). The PRI formulations proposed in this
293 study (Table 4) were based on the results obtained in previous work (Gamon *et al.*, 1993;
294 Rouse *et al.*, 1974; Jordan, 1969) and on the spectral trend of the reflectance at the 500-600
295 nm region. Figure 4a shows the needle spectral reflectance of *Pinus sylvestris* measured
296 with a Unispec spectroradiometer for two stress levels at 12:00 GMT. As shown in Figure
297 4b both regions at 500-520 nm and 570-590 nm could be used as a reference band. Figure
298 4b also shows the bandwidth corresponding to AHS airborne sensor used to calculate
299 PRI_{570} and PRI_{512} .

300 The indices were also normalized by structure-sensitive effects using indices such as NDVI
301 (Rouse *et al.*, 1974), SR (Jordan, 1969; Rouse *et al.*, 1974), MTVI2 (Haboudane *et al.*,
302 2004), OSAVI (Rondeaux *et al.*, 1996) and MSAVI (Haboudane *et al.*, 2004). Indices were
303 adapted to the AHS bandset using the closest bands available.

304

305 **2.5. Model simulation with LIBERTY and INFORM**

306 Radiative transfer modeling methods were applied with the *Leaf Incorporating*
307 *Biochemistry Exhibiting Reflectance and Transmittance Yields* (LIBERTY) model (Dawson
308 *et al.*, 1998) linked to the *Invertible Forest Reflectance Model* (INFORM) (Atzberger,
309 2000). LIBERTY was designed to model conifer (particularly pine) needles at the cellular

310 scale, based on Melamed's radiative transfer theory of powders (Melamed, 1963). This
311 model calculates reflectance and transmittance by assuming the needle structure to be cell
312 spheres separated by air gaps. The LIBERTY and PROSPECT models were assessed by
313 Zarco-Tejada *et al.* (2004) and Moorthy *et al.* (2008) suggesting that PROSPECT could be
314 used to model needle optical properties. PROSPECT is a radiative model initially designed
315 for broad leaves, although it was later adapted to needles (Malenovsky *et al.*, 2006). In a
316 recent paper, Di Vittorio (2009) enhanced the limitation of LIBERTY to resolve individual
317 pigments and the gaps in the estimation of *in vivo* specific absorption coefficients and
318 model biophysics. At canopy level, INFORM simulates the *bi-directional* reflectance of
319 forest stands between 400 and 2500 nm, being a combination of the *Forest Light*
320 *Interaction Model* (FLIM) (Rosema *et al.*, 1992) and *Scattering by Arbitrarily Inclined*
321 *Leaves* (SAILH) (Verhoef, 1984, 1985), coupled with LIBERTY for this study. Neither
322 FLIM nor INFORM incorporates a correction to account for the fact that, in coniferous
323 forests, needles are densely clumped into shoots. Such correction has been suggested by
324 Nilson and Ross (1997) and Smolander and Stenberg (2003). However, INFORM is an
325 innovative hybrid model with crown transparency, infinite crown reflectance and
326 understory reflectance simulated using physically based sub-models. Hybrid models are
327 combinations of geometrical and turbid medium models, therefore with INFORM tree
328 crowns are not considered opaque but rather treated as a turbid medium. This factor plays
329 an important role in conifer Mediterranean forests characterized by heterogeneous
330 structures, thin leafy canopies and mutually shaded crowns.

331

332 A total of 125 simulations were performed with the LIBERTY+INFORM coupled model,
333 varying LAI (1-3), tree density (800-2800 trees/ha), and chlorophyll concentration (100-

334 500 mg/m²). The simulated spectral reflectance dataset was used to calculate the vegetation
335 indices under analysis: PRI₅₇₀, modified PRI formulations, and PRI indices normalized by
336 the NDVI, SR, OSAVI, MSAVI and MTVI2 structural indices (Table 4). Model
337 simulations were conducted for each PRI formulation to assess the effects of the reference
338 band on PRI. The purpose of the simulation analysis was to assess the effects of the
339 variability found in a pine forest on the simulated PRI formulations as a function of i) LAI;
340 ii) fractional cover; and iii) Cab concentration. Model assessments and comparison against
341 ground-measured EPS both at leaf and canopy levels were conducted.

342

343 **3. Results**

344 **3.1. Model simulations**

345 Model simulations conducted with LIBERTY for *Pinus nigra* needles using the
346 PROSPECT chlorophyll absorption coefficient (k_{ab}) revealed good agreement when
347 compared with needle spectra measured with the integrating sphere (Figure 5). In contrast,
348 LIBERTY simulations conducted with the original chlorophyll absorption coefficient
349 (Dawson *et al.*, 1998) reported a significant failure to match the needle reflectance
350 measured in the 500-700 nm region (Figure 5a and 5b). Input parameters and ranges used
351 for the coupled LIBERTY+INFORM model (Table 5) were estimated by the inversion of
352 128 needle spectra measured in the laboratory with the integrating sphere for both species.
353 At the canopy level, the coupled model was assessed against the reflectance extracted from
354 the AHS data for study areas from both species. Figure 5c shows good agreement between
355 the reflectance spectra obtained from the AHS image and those simulated with the
356 LIBERTY+INFORM coupled model for one of the study areas.

357

358 The LIBERTY+INFORM coupled model was used to assess the effects of canopy
359 architecture on PRI and on the proposed PRI formulations (Table 4). A comparison
360 between the coefficient of variation (CV) for each PRI reference band was conducted to
361 assess the PRI formulation showing less variation as a function of LAI, tree density and
362 chlorophyll content. Figure 6 shows the mean, the CV, and the standard deviation of
363 simulated spectral reflectance for a range of LAI and tree densities. The simulations were
364 conducted for LAI values of 1 to 3, and tree densities in the range 800 - 2800 trees/ha. The
365 remaining inputs were set to the mean nominal values (Table 5). The CV obtained from
366 each reference band (R_{512} , R_{570} , R_{600} and R_{670}) was 4.35%, 5.28%, 5.02% and 13.52%,
367 respectively. Although the differences among the CV of the reference bands were no
368 greater than 15%, R_{512} had the lowest value (Figure 6). However, such differences
369 increased when calculating the CV for PRI formulations, yielding CV=48.98% for PRI_{570}
370 and CV=22.05% for PRI_{512} , demonstrating that PRI_{570} had a higher variation than other PRI
371 formulations such as PRI_{512} . These theoretical results suggest that PRI_{512} is less sensitive to
372 changes in LAI and tree densities than PRI_{570} . The effect of chlorophyll concentration was
373 also studied by simulating a range of chlorophyll (100-500 mg/m²), in addition to the
374 variation in LAI (1-3) and tree density (800-2800 trees/ha). In this case, the CV for PRI_{570}
375 decreased slightly (CV=30.48%), while PRI_{512} remained almost invariant (CV=23.01%).
376 These results suggest that PRI_{512} is less sensitive to structural parameters and chlorophyll
377 variations than PRI_{570} .

378

379 The structural effects on PRI formulations are shown as normalized for LAI=1 (Figure 7),
380 showing the variation in PRI_{570} and PRI_m for a range of LAI and tree densities (Figure 7 a,
381 b, c and d). The variation in PRI_{m1} and PRI_{m4} was less significant than that of the rest of the

382 PRI formulations (PRI₅₇₀, PRI_{m2}, PRI_{m3}). Such differences were even greater when tree
383 density or LAI increased. The patterns tracked by PRI₅₇₀ versus PRI_{m1} as simulated for a
384 range of LAI and tree density values (Figure 8) demonstrates the lower sensitivity of PRI_{m1}
385 to canopy structural changes than PRI₅₇₀. These results demonstrate the smaller effect
386 caused by the tree density on PRI₅₁₂ as compared to PRI₅₇₀.

387 Model simulations for canopy PRI₅₇₀ and PRI_m indices were also conducted with
388 LIBERTY+INFORM for assessing index variation as a function of chlorophyll
389 concentration (Figure 9). Simulations performed for increasing tree densities (Figure 9a
390 (800 trees/ha); 9b (1300 trees/ha); 9c (1800 trees/ha)) as a function of LAI and Cab
391 demonstrate that PRI₅₇₀ and PRI_{m1} are affected by Cab.

392 **3.2. Experimental results**

393 **3.2.1. PRI measurements at the needle level**

394 The assessment to study the relationship between PRI₅₇₀ and the epoxidation state of the
395 xanthophylls pigments (EPS) was conducted on the diurnal dataset acquired at the leaf
396 level. The comparison between EPS at 8:00 and 12:00 GMT for *Pinus sylvestris* (Figure
397 10a) and *Pinus nigra* (Figure 10b) for each study area demonstrates the differences found
398 on EPS as a function of the stress level. There were significant differences in EPS between
399 study areas for both species at 12:00 GMT. Values were not significantly different at 8:00
400 GMT for *P. sylvestris* and *P. nigra*. However, both species displayed a similar pattern, as
401 diurnal differences in EPS increased on the areas with higher stress.

402 Based on midday measurements, EPS showed a consistent pattern of decline on needle
403 PRI₅₇₀ and needle PRI₅₁₂ data at 10 and 30nm bandwidths for both *Pinus sylvestris* (Figure
404 11) and *Pinus nigra* sites (Figure 12). Results demonstrated a similar sensitivity of both
405 PRI₅₇₀ and PRI₅₁₂ to EPS, yielding coefficients of determination of $r^2=0.61$ for PRI₅₇₀

406 (Figure 11a) and $r^2=0.59$ for PRI₅₁₂ (Figure 11b) for *Pinus sylvestris*, and $r^2=0.62$ for
407 PRI₅₇₀ (Figure 12a) and $r^2=0.61$ for PRI₅₁₂ (Figure 12b) for *Pinus nigra*. A higher
408 concentration of the photosynthetic active pigment violaxanthin over the whole xanthophyll
409 pool corresponds with higher values of EPS, and consequently smaller stress levels, thus
410 showing lower PRI values. Similar results were found at the leaf level in *Abies alba*
411 (Peguero-Pina *et al.*, 2007) and *Pinus sylvestris* (Filella *et al.*, 2009) needles, and in
412 *Quercus coccifera* (Peguero-Pina *et al.*, 2008) and *Prunus persica* (Suárez *et al.*, 2010)
413 leaves.

414

415 The PRI formulations were then calculated for a FWHM of 30nm, simulating the airborne
416 AHS sensor bandwidth. Results showed significant relationships between EPS and indices
417 PRI₅₇₀ and PRI₅₁₂ for *P. sylvestris* and *P. nigra* (Figures 11 and 12). The coefficients of
418 determination obtained for both species were similar, $r^2=0.59$ for PRI₅₇₀ (Figure 11c) and
419 $r^2=0.40$ for PRI₅₁₂ (Figure 11d) for *Pinus sylvestris*, and $r^2=0.59$ for PRI₅₇₀ (Figure 12c) and
420 $r^2=0.57$ for PRI₅₁₂ (Figure 12d) for *Pinus nigra*. The comparison of the relationships
421 obtained with a FWHM of 10 and 30 nm (Figures 11 and 12) shows that the instrument
422 FWHM affects the relationships between PRI and EPS, as expected. Nevertheless, results
423 obtained at 30nm FWHM yielded significant relationships between EPS and both PRI₅₇₀
424 and needle PRI₅₁₂. Consistent relationships were also obtained when aggregating the needle
425 spectra at the plot level using the FWHM of the airborne AHS sensor (later used to acquire
426 the imagery). Results of these relationships are shown in Figure 13, yielding coefficients of
427 determination of $r^2=0.89$ for EPS vs PRI₅₇₀ (Figure 13a) and $r^2=0.73$ for EPS vs PRI₅₁₂
428 (Figure 13b).

429

430 **3.2.2. Results for PRI formulations at the canopy level.**

431 The study conducted to assess the relationships between field-measured EPS and
432 crown-level PRI indices was conducted by selecting pixels with NDVI higher than 0.6 from
433 windows of 3x3 pixels with center on the targeted crown. Vegetation indices assessed were
434 PRI_{570} , and modified PRI formulations (PRI_{m1} , PRI_{m2} , PRI_{m3} , PRI_{m4}), as well as the
435 normalized modified PRI_{m1} indices over structural vegetation indices NDVI, SR, OSAVI,
436 MSAVI and $MTVI_2$. Results showed that the airborne-level PRI indices were sensitive to
437 EPS but, as expected were also highly affected by structural parameters. The relationships
438 between EPS and indices PRI_{570} , PRI_{512} , NDVI and T are shown in Figure 14. The index
439 PRI_{512} shows higher relationships with EPS ($r^2=0.40$) than PRI_{570} ($r^2=0.21$) (Figure 14a and
440 b), demonstrating with the EPS vs NDVI relationship that structural effects due to stress
441 were not the major driver (Figure 14c) ($r^2=0.13$). Significant relationships were also found
442 between T and EPS, although with lower coefficient of determination ($r^2=0.37$) (Figure
443 14d). These results show that the relationship between PRI_{512} and EPS was stronger than
444 with PRI_{570} . In agreement with the modeling results obtained, results show that PRI_{570}
445 might be more affected by structural effects than PRI_{512} . According to the modeling results
446 presented in Figure 7, the PRI_{512} index seems less affected by structural effects than the
447 PRI_{570} index for high tree densities (Fig. 7c and 7d) and slightly less or equally affected for
448 low tree densities (Fig. 7a and 7b). Moreover, the normalized results (Figure 8) show less
449 LAI effects on PRI_{512} as compared to PRI_{570} . Besides the mentioned structural effects, clear
450 differences can be seen between both indices under varying chlorophyll content (Fig. 9)
451 where the pigment effects were smaller for PRI_{512} . In the field study, structural effects on
452 the indices were further restricted by selecting pixels with $NDVI>0.6$, therefore targeting
453 pure vegetation pixels and limiting the variation of the canopy structure. Under these

454 conditions, the experimental results suggested a greater robustness of PRI₅₁₂ for both
455 canopy structure (tree density and LAI) and chlorophyll content variation.

456 Crown-level relationships also showed significant coefficients of determination between
457 PRI₅₁₂ and field-measured indicators of water stress such as Gs, ($r^2=0.45$) and Ψ , ($r^2=0.48$)
458 (Figure 15). In comparison, PRI₅₇₀ yielded a coefficient of determination of $r^2=0.21$ (Gs)
459 and $r^2=0.21$ (Ψ). These results demonstrate that PRI₅₁₂ might be used as an indicator of
460 water stress in conifer forest, and demonstrate the consistency with previously presented
461 modeling results. Furthermore, these results are in agreement with the canopy results
462 between EPS and PRI₅₁₂, which shows a superior performance for PRI₅₁₂. Other index
463 modifications for PRI, such as PRI_{m2}, PRI_{m3} and PRI_{m4}, were shown to be very sensitive to
464 structural parameters (data not included). The study conducted to assess the effects of
465 normalizing PRI by structural vegetation indices such as NDVI, SR, OSAVI and MSAVI
466 indicated little improvement (data not included).

467

468 PRI₅₇₀, PRI_{m1} and NDVI were applied at the image level to map stress over the study areas.
469 Figure 16 shows the three *Pinus nigra* study areas (SN1, SN2, SN3) and two zoomed
470 images of each central plot at 1x1 and 3x3 resolution (pixel based) and at object level. A
471 visual analysis reveals that the study areas with different stress levels showed similar NDVI
472 and PRI₅₇₀ values, but different PRI₅₁₂ values (Figure 16). To quantify these differences the
473 mean and the standard deviation for each index were calculated for the four trees displayed
474 in the zoom images (Figure 16), for a total of twelve trees for each species. While the mean
475 values for NDVI and PRI₅₇₀ were similar among the study areas, PRI₅₁₂ showed different
476 ranges for each stress level (Figure 17a). A similar comparison was conducted for *Pinus*
477 *sylvestris* (Figure 17b). Simulation and experimental results were consistent with the

478 mapping results obtained for PRI₅₁₂, showing its ability for accurately mapping stress at
479 both pixel and object levels in conifer forests.

480

481

482

483 **5. Conclusions**

484 Radiative transfer simulation methods were applied using INFORM as a canopy reflectance
485 model linked with a modified LIBERTY leaf model in order to assess the effects of canopy
486 structure on different formulations of PRI. The simulations were conducted by computing
487 canopy reflectance spectra with different values of LAI, tree density and chlorophyll
488 content, assessing the effects of these biochemical and structural inputs on the proposed
489 PRI formulations. The study demonstrated the sensitivity of PRI and modified PRI indices
490 to canopy structural parameters and, therefore, the need for assessing robust PRI
491 formulations with less structural effects. The simulation results demonstrate that PRI₅₁₂ is
492 less sensitive to changes in LAI values, tree densities and chlorophyll content than PRI₅₇₀.

493

494 In addition to the simulation work conducted, PRI indices were also tested using
495 experimental data collected from the study sites at 8:00 and 12:00 GMT. Significant
496 differences for both species were found in EPS measured at 12:00 GMT as a function of the
497 stress levels, showing that EPS declined consistently with PRI₅₇₀ and PRI₅₁₂. At the leaf
498 level, both PRI₅₇₀ and PRI₅₁₂ were sensitive to EPS measured by destructive sampling.
499 Nevertheless, the study conducted at the canopy level revealed that PRI₅₁₂ was better
500 correlated with EPS and physiological indicators, such as water potential and stomatal
501 conductance, than PRI₅₇₀. The better performance obtained for PRI₅₁₂ over PRI₅₇₀ at the

502 canopy level in the experimental study confirms the modeling results which showed the
503 lower sensitivity of PRI₅₁₂ to structural effects in conifer canopies as compared to PRI₅₇₀.
504 Other formulations such as PRI_{m2}, PRI_{m3} and PRI_{m4} were highly sensitive to structural
505 parameters and therefore not optimum for stress detection in these canopies. The sensitivity
506 of the PRI indices to structural parameters is critical in conifer forests, where the
507 heterogeneity allows greater influence due to the ground layer and shadows.

508

509 This work demonstrates the link between PRI₅₁₂ and PRI₅₇₀ with EPS in *P. sylvestris* and *P.*
510 *nigra* at the leaf level, and it suggests the superior performance at the canopy level for
511 PRI₅₁₂ versus PRI₅₇₀ when mapping previsual stress levels in conifer forests.

512

513

514

515 **Acknowledgements**

516 Financial support from EGMASA (Environmental Management Company, Ltd.) and the
517 Environmental Ministry of the Regional Andalusian Government, and partial support from
518 the Innovation and Development Agency of Andalusia (Regional Ministry of Innovation,
519 Science and Enterprise), are gratefully acknowledged, as well as support from the
520 GESBOME project (Regional Andalusian Government P06-RNN-1890) and Aragón
521 Government (A03 research group). J. E. Frieyro de Lara, A. Hayas-López, Rafael Sánchez
522 and David Ariza are acknowledged for measurements and technical support in the field
523 campaigns, and A. Calviño for technical help with the HPLC measurements. J. E. Granados
524 and the members of CAHA (German-Spanish Astronomical Center at Calar Alto),

525 Eustaquio Gil-Pelegrín and J. J. Peguero-Pina (CITA, Zaragoza) are acknowledged for
526 technical support.

527

528 **References**

529 Abadía, A. & Abadía, J. (1993). Iron and plant pigments. In L. L. Barton & B. C. Hemming
530 (Eds.), *Iron Chelation in Plants and Soil Microorganisms* (pp. 327-344). Academic: San
531 Diego.

532

533 Asner, G. P., Carlson, K. M., & Martin, R. E. (2005). Substrate age and precipitation
534 effects on Hawaiian forest canopies from spaceborne imaging spectroscopy. *Remote*
535 *Sensing of Environment*, 98, 457-467.

536

537 Allen C. D., Macalady A. K., Chenchouni H., Bachelet D., McDowell N., Vennetier M.,
538 Kitzberger T., Rigling A., Breshears D. D., Hogg E. H., Gonzalez P., Fensham R., Zhang
539 Z., Castro J., Demidova N., Lim J. H., Allard G., Running S.W., Semerci A. & Cobb N.
540 (2009). A global overview of drought and heat-induced tree mortality reveals emerging
541 climate change risks for forests. *Forest Ecology and Management*, 259, 660-684.

542

543 Atzberger, C. (2000). Development of an invertible forest reflectance model: The INFOR-
544 Model. In: Buchroithner (Ed.), *A Decade of Trans-European Remote Sensing Cooperation*.
545 Proceedings of the 20th EARSeL Symposium, Dresden, Germany, 14-16 June 2000, pp.
546 39-44.

547

548 Barton, C. V. M. & North, P. R. J. (2001). Remote sensing of canopy light use efficiency
549 using the Photochemical Reflectance Index. Model and analysis. *Remote Sensing of*
550 *Environment*, 78, 264-273.

551

552 Berk, A., Anderson, G. P., Acharya, P. K., Chetwynd, J. H., Bernstein, L. S., Shettle, E. P.,
553 Matthew, M. W., and Adler-Golden, S. M. (2000). *MODTRAN4 User's Manual*, Air Force
554 Research Laboratory, Hanscom MA.

555

556 Berk A., Bernstein L. S., Anderson G. P., Acharya P. K., Robertson D. C., Chetwynd J. H.
557 & Adler-Golden S. M. (1998). MODTRAN cloud and multiple scattering upgrades with
558 application to AVIRIS. *Remote Sensing of Environment*, 65, 367-375.

559

560 Berni, J. A. J., Zarco-Tejada, P. J., Sepulcre-Cantó, G., Fereres, E., & Villalobos, F. J.
561 (2009). Mapping stomatal conductance and CWSI in olive orchards using high resolution
562 thermal remote sensing imagery. *Remote Sensing of Environment*, 113, 2380-2388.

563

564 Björkman, O. & Demmig-Adams, B. (1994). Regulation of photosynthetic light energy
565 capture, conversion, and dissipation in leaves of higher plants. In: Schulze DE & MM
566 Caldwell (Eds.), *Ecophysiology of Photosynthesis* (pp. 17-45). Springer-Verlag, Berlin,
567 Germany.

568

569 Dawson, T. P., Curran P. J. & Plummer S. E. (1998). LIBERTY - Modelling the Effects of
570 Leaf Biochemical Concentration on Reflectance Spectra. *Remote Sensing of Environment*,
571 65, 50-60.
572

573 Demmig-Adams B. & Adams W. W. (1996). The role of xanthophyll cycle carotenoids in
574 the protection of photosynthesis. *Trends in Plant Science*, 1, 21-26.
575

576 Di Vittorio A. V. (2009). Enhancing a leaf radiative transfer model to estimate
577 concentrations and *in vivo* specific absorption coefficients of total carotenoids and
578 chlorophylls *a* and *b* from single-needle reflectance and transmittance.
579 *Remote Sensing of Environment*, 113, 1948-1966.
580

581 Drolet, G. G., Huemmrich, K. F., Hall, F. G., Middleton, E. M., Black, T. A., Barr, A. G. &
582 Margolis, H. A. (2005). A MODIS-derived Photochemical Reflectance Index to detect
583 inter-annual variations in the photosynthetic light-use efficiency of a boreal deciduous
584 forest. *Remote Sensing of Environment*, 98, 212-224.
585

586 Ferretti M. (1994). *Especies forestales mediterráneas. Guía para la evaluación de las*
587 *copas*. CEE-UN/ECE. Bruselas, Ginebra.
588

589 Filella, I., Amaro, T., Araus, J. L., & Peñuelas, J. (1996). Relationship between
590 photosynthetic radiation-use efficiency of barley canopies and the photochemical
591 reflectance index (PRI). *Physiologia Plantarum*, 96, 211-216.
592

593 Filella, I., Porcar-Castell, A., Munné-Bosch, S., Bäck, J. M., Garbulsky F. & Peñuelas, J.
594 (2009). PRI assessment of long-term changes in carotenoids/chlorophyll ratio and short-
595 term changes in de-epoxidation state of the xanthophyll cycle. *Remote Sensing of*
596 *Environment*, 30, 4443-4455.
597

598 Gamon, J. A., Filella, I., and Peñuelas, J. (1993). The dynamic 531nm reflectance signal: A
599 survey of twenty angiosperm species. In: Yamamoto, H.Y. and Smith, C.M., Editors, 1993.
600 Photosynthetic responses to the environment. *American Society of Plant Physiologists*,
601 Rockville, MD, pp. 172-177.
602

603 Gamon, J. A., Serrano, L. and Surfus, J. S. (1997). The photochemical reflectance index: an
604 optical indicator of photosynthetic radiation use efficiency across species, functional types
605 and nutrient levels. *Oecologia* 112, 492-501.
606

607 Gamon, J. A., Peñuelas, J., & Field, C. B. (1992). A narrow-waveband spectral index that
608 tracks diurnal changes in photosynthetic efficiency. *Remote Sensing of Environment*, 41,
609 35-44.
610

611 Garbulsky, M. F., Peñuelas, J., Papale, D., & Filella, I. (2008). Remote estimation of
612 carbon dioxide uptake by a Mediterranean forest. *Global Change Biology*, 14, 2860-2867.
613

614 Haboudane D., Miller J. R., Pattey E., Zarco-Tejada P. J. & Strachan I. B. (2004).
615 Hyperspectral vegetation indices and novel algorithms for predicting green LAI of crop

616 canopies: Modeling and validation in the context of precision agriculture. *Remote Sensing*
617 *of Environment*, 90, 337-352.

618

619 Hall, F. G., Hilker, T., Coops, N. C., Lyapustin, A., Huemmrich, K. F., Middleton, E. M.,
620 Margolis, H. A., Drolet, G. G., & Black, T. A. (2008). Multi-angle remote sensing of forest
621 light use efficiency by observing PRI variation with canopy shadow fraction. *Remote*
622 *Sensing of Environment*, 112, 3201-3211.

623

624 Heikkilä, J., Nevalainen S. & Tokola T. (2002). Estimating defoliation in boreal coniferous
625 forests by combining Landsat TM, aerial photographs and field data. *Forest Ecology and*
626 *Management*, 158, 9-23.

627

628 Hilker T., Coops N. C., Hall F. G., Black T. A., Wulder M. A., Nestic Z. & Krishnan P.
629 (2008). Separating physiologically and directionally induced changes in PRI using BRDF
630 models. *Remote Sensing of Environment*, 112, 2777-2788.

631

632 Hilker T., Lyapustin A., Hall F. G., Wang Y., Coops N. C., Drolet G., & Black T. A.
633 (2009). An assessment of photosynthetic light use efficiency from space: Modeling the
634 atmospheric and directional impacts on PRI reflectance. *Remote Sensing of Environment*,
635 113, 2463-2475.

636

637 Inoue, Y., Peñuelas, J., Miyata A., & Mano, M. (2008). Normalized difference spectral
638 indices for estimating photosynthetic efficiency and capacity at a canopy scale derived from
639 hyperspectral and CO₂ flux measurements in rice. *Remote Sensing of Environment*, 112,
640 156-172.

641

642 Jackson, R. D., Reginato, R. J., & Idso, S. B. (1977). Wheat canopy temperature: A
643 practical tool for evaluating water requirements. *Water Resources Research*, 13, 651-656.

644

645 Jordan, C. F. (1969). Derivation of leaf area index from quality of light on the forest floor.
646 *Ecology*, 50, 663-666.

647

648 Larbi, A., Abadía, A., Morales, F., & Abadía, J. (2004). Fe resupply to Fe-deficient sugar
649 beet plants leads to rapid changes in the violaxanthin cycle and other photosynthetic
650 characteristics without significant *de novo* chlorophyll synthesis. *Photosynthesis Research*,
651 79, 59-69.

652

653 Martínez-Vilalta J., López B. C., Adell N., Badiella L. & Ninyerola M. (2008). Twentieth
654 century increase of Scots pine radial growth in NE Spain shows strong climate interactions.
655 *Global Change Biology*, 14, 2868-2881.

656

657 Malenovsky Z., Albrechtova J., Lhotakova Z., Zurita-Milla R., Clevers G. P. W.,
658 Schaepman M. E., & Cudlín P. (2006). Applicability of the PROSPECT model for Norway
659 spruce needles. *International Journal of Remote Sensing*, 27, 5315-5340.

660

661 Melamed N. T. (1963). Optical properties of powders. Part I. Optical absorption
662 coefficients and the absolute value of the diffuse reflectance. Part II. Properties of
663 luminescent powders, *Applied Optics*, 34, 560-570.
664

665 Melzack, R. N., Bravdo B. & Riov J. (1985). The effect of water stress on photosynthesis
666 and related parameters in *Pinus halepensis*. *Physiologia Plantarum*, 64, 295-300.
667

668 Middleton E.M., Cheng Y.B., Hilker T., Black T.A., Krishnan P., Coops N.C. &
669 Huemmrich K.F. (2009). Linking foliage spectral responses to canopy level ecosystem
670 photosynthetic light use efficiency at a Douglas-fir forest in Canada. *Canadian Journal of*
671 *Remote Sensing*, 35, 166-188.
672

673 Moorthy I., Miller J. R., & Noland T. L. (2008). Estimating chlorophyll concentration in
674 conifer needles with hyperspectral data: An assessment at the needle and canopy level.
675 *Remote Sensing of Environment*, 112, 2824-2838.
676

677 Navarro-Cerrillo, R. M., Varo, M. A., Lanjeri, S., & Hernández-Clemente, R. (2007).
678 Cartografía de defoliación en los pinares de pino silvestre (*Pinus sylvestris* L.) y pino
679 salgareño (*Pinus nigra* Arnold) en la Sierra de los Filabres. *Ecosistemas*, 16, 163-171.
680

681 Nilson, T. & Ross, J. (1997). Modeling radiative transfer through forest canopies:
682 Implications for canopy photosynthesis and remote sensing. In: H. L. Gholz, K. Nakane,
683 and H. Shimoda (Eds.), *The Use of Remote Sensing in the Modeling of Forest Productivity*
684 (pp. 23-60). Kluwer, Dordrecht.
685

686 Peguero-Pina, J. J., Camarero, J. J., Abadía, A., Martín, E., González-Cascón, R., Morales,
687 F., & Gil-Pelegrín. (2007). Physiological performance of silver-fir (*Abies alba* Mill.)
688 populations under contrasting climates near the south-western distribution limit of the
689 species. *Flora*, 202, 226-236.
690

691 Peguero-Pina, J. J., Morales, F., Flexas, J., Gil-Pelegrín, E., & Moya, I. (2008).
692 Photochemistry, remotely sensed physiological reflectance index and de-epoxidation state
693 of the xanthophyll cycle in *Quercus coccifera* under intense drought. *Oecologia*, 156, 1-11.
694

695 Peñuelas, J., Filella, I., and Gamon, J. A. (1995). Assessment of photosynthetic radiation
696 use efficiency with spectral reflectance. *New Phytologist*, 131, 291- 296.
697

698 Peñuelas, J., J. A. Gamon, A. L. Fredeen, Merino J. & Field C. B. (1994). Reflectance
699 indices associated with physiological changes in nitrogen- and water-limited sunflower
700 leaves. *Remote Sensing of Environment*, 48, 135-146.
701

702 Poyatos R.; Llorens P.; Piñol J. & Rubio C. (2008). Response of Scots pine (*Pinus*
703 *syvestris* L.) and pubescent oak (*Quercus pubescens* Willd.) to soil and atmospheric water
704 deficits under Mediterranean mountain climate. *Annals of Forest Science*, 65, 306.
705

706 Qi, J., Chehbouni A., Huete A. R., Kerr Y. H. (1994). Modified Soil Adjusted Vegetation
707 Index (MSAVI). *Remote Sensing of Environment*, 48, 119-126.

708
709 Rebetz M. & Dobbertin M. (2004). Climate change may already threaten Scots pine stands
710 in the Swiss Alps. *Theoretical and Applied Climatology*, 79, 1-9.
711
712 Richardson, A. D. & Berlyn, P. (2002). Changes in foliar spectral reflectance and
713 chlorophyll fluorescence of four temperate species following branch cutting. *Tree*
714 *Physiology*, 22, 499-506.
715
716 Rondeaux, G., Steven, M., & Baret, F. (1996). Optimization of soil-adjusted vegetation
717 indices. *Remote Sensing of Environment*, 55, 95-107.
718
719 Rouse, J. W., Haas, R. H., Schell, J. A., Deering, D. W. & Harlan, J. C. (1974). Monitoring
720 the Vernal Advancement and Retrogradation (Greenwave Effect) of Natural Vegetation.
721 Type III Final Report, NASA Goddard Space Flight Center, Greenbelt, Maryland, 20771,
722 USA, 371 pp.
723
724 Rosema A., W. Verhoef, H. Noorbergen & Borgesius J. J. (1992). A new forest light
725 interaction model in support of forest monitoring. *Remote Sensing of Environment*, 42, 23-
726 41.
727
728 Schlerf, M., Atzberger, C. G. & Hill, J. (2005). Remote sensing of forest biophysical
729 variables using HyMap imaging spectrometer data. *Remote Sensing of Environment*,
730 95, 177-194.
731
732 Schlerf, M. & Atzberger, C. G. (2006). Inversion of a forest reflectance model to estimate
733 structural canopy variables from hyperspectral remote sensing. *Remote Sensing of*
734 *Environment*, 100, 281-294.
735
736 Scholander, P. F.; Hammel, H. T.; Bradstreet, E. D.; Hemmingsen, E.A. (1965). Sap
737 pressure in vascular plants. *Science*, 148, 339-346.
738
739 Sepulcre-Cantó, G., Zarco-Tejada, P. J., Jiménez-Muñoz, J. C., Sobrino, J. A., de Miguel,
740 E., & Villalobos, F. J. (2006). Detection of Water Stress in an Olive Orchard with Thermal
741 Remote Sensing Imagery. *Agricultural and Forest Meteorology*, 136, 31-44.
742
743 Sepulcre-Cantó, G., Zarco-Tejada, P. J., Jiménez-Muñoz, J. C., Sobrino, J. A., Soriano, M.
744 A., Fereres, E., Vega, V., & Pastor, M. (2007). Monitoring yield and fruit quality
745 parameters in open-canopy tree crops under water stress. Implications for ASTER. *Remote*
746 *Sensing of Environment*, 107, 455-470.
747
748 Sepulcre-Cantó, G., Zarco-Tejada, P. J., Sobrino, J. A., Berni, J. A. J., Jiménez Muñoz, J.
749 C., & Gastellu-Etchegorry, J. P. (2009). Detecting water status in open canopies with
750 thermal ASTER imagery and DART radiative transfer simulation. *Agricultural and Forest*
751 *Meteorology*, 149, 962-975.
752

753 Sims, D. A. & Gamon, J. A. (2002). Relationships between leaf pigment content and
754 spectral reflectance across a wide range of species, leaf structures and developmental
755 stages. *Remote Sensing of Environment*, 81, 337-354.

756
757 Smolander S. & Stenberg P. (2003). A method to account for shoot scale clumping in
758 coniferous canopy reflectance models. *Remote Sensing of Environment*, 88, 363-373.

759
760 Sobrino, J. A., Jiménez-Muñoz, J. C., Labeled-Nachbrand, J. & Nerry F. (2002). Surface
761 emissivity retrieval from Digital Airborne Imaging Spectrometer data. *Journal of*
762 *Geophysical Research*, 107, (D23), 4729, doi: 10.1029/2002JD002197.

763
764 Sobrino, J. A., Jiménez-Muñoz, J. C., Zarco-Tejada, P. J., Sepulcre-Cantó, G. & de Miguel,
765 E. (2006). Land Surface Temperature derived from Airborne Hyperspectral Scanner
766 Thermal Infrared data. *Remote Sensing Environment*, 102, 99–115.

767
768 Suárez, L., Zarco-Tejada, P. J., Sepulcre-Cantó, G., Pérez-Priego, O., Miller, J. R.,
769 Jiménez-Muñoz, J. C., Sobrino, J. (2008). Assessing Canopy PRI For Water Stress
770 Detection With Diurnal Airborne Imagery. *Remote Sensing of Environment*, 112, 560-575.

771
772 Suárez, L., Zarco-Tejada, P. J., Berni, J. A. J., González-Dugo, V., Fereres, E. (2009).
773 Modelling PRI for Water Stress Detection using Radiative Transfer Models. *Remote*
774 *Sensing of Environment*, 113, 730-744.

775
776 Suárez, L., Zarco-Tejada, P. J., González-Dugo, V., Berni, J. A. J., Sagardoy, R., Morales,
777 F., Fereres, E. (2010). Detecting water stress effects on fruit quality in orchards with time-
778 series PRI airborne imagery. *Remote Sensing of Environment*, 114, 286-298.

779
780 Thayer, S. S. & Björkman, O. (1990). Leaf xanthophyll content and composition in sun
781 and shade determined by HPLC. *Photosynthesis Research*, 23, 331-343.

782
783 UN/ECE, (1994). Manual on Methods and Criteria for Harmonised Sampling, Assessment,
784 Monitoring and Analysis of the Effects of Air Pollution on Forests. *Third ed. Programme*
785 *Co-ordinating Centres*, Hamburg and Prague. [http://www.icp-](http://www.icp-forests.org/pdf/FINAL_Crown.pdf)
786 [forests.org/pdf/FINAL_Crown.pdf](http://www.icp-forests.org/pdf/FINAL_Crown.pdf)

787
788 Verhoef, W. (1984). Light scattering by leaf layers with application to canopy reflectance
789 modeling: The SAIL model. *Remote Sensing of Environment*, 16, 125-141.

790
791 Verhoef, W. (1985). Earth observation modeling based on layer scattering matrices. *Remote*
792 *Sensing of Environment*, 17, 165-178.

793
794 Yamamoto, Y. (1979). Biochemistry of the violaxanthin cycle in higher plants, *Pure &*
795 *Applied Chemistry*, 51, 639-648.

796
797 Zarco-Tejada, P. J., Miller, J. R., Harron, J., Hu, B., Noland, T. L., Goel, N., Mohammed
798 G. H. & Sampson, P. H. (2004). Needle chlorophyll content estimation through model

799 inversion using hyperspectral data from boreal conifer forest canopies. *Remote Sensing of*
800 *Environment*, 89, 189-199.

801

802 Zhang, Y., Chen, J. M., Miller, J. R., & Noland, T. L. (2008). Retrieving chlorophyll
803 content of conifer needles from hyperspectral measurements. *Canadian Journal of Remote*
804 *Sensing*, 34, 296-310.

805

806

807

Table 1. Structural parameters of *Pinus nigra* and *Pinus sylvestris* forest in the training areas. Mean values of age, height, basimetric area (BA) and min and max values of density.

Main species (Units)	Age (years)	Height (m)	Density (trees ha ⁻¹)	BA (m ² ha ⁻¹)
<i>Pinus sylvestris</i> L.	35	7.99	1100-1895 (Mean: 1475)	26.55
<i>Pinus nigra</i> Arnold	40	8.60	950-2263 (Mean:1594)	27.33

Table 2. Mean values and standard deviation of structural parameters calculated from the twelve trees measured in each study area for *Pinus sylvestris* (SS1, SS2, SS3) and *Pinus nigra* (SN1, SN2, SN3). Mean values of defoliation (%), basimetric area (BA), perimeter, height, stem height, trunk longitude, crown diameter and leaf area index (LAI).

Study area	BA (m ² ha ⁻¹)	Perimeter (cm)	Height (m)	Stem height (m)	Trunk long. (m)	Crown diameter (m)	LAI
SS1	27.67 (±3.78)	49.61 (± 5.42)	8.71 (± 0.93)	2.16 (± 1.72)	0.47 (± 0.02)	3.13 (± 0.74)	2.25 (± 0.02)
SS2	22.00 (±7)	48.33 (± 4.47)	7.97 (±0.49)	2.17 (± 0.147)	0.64 (± 0.01)	3.12 (± 0.41)	2.36 (± 0.46)
SS3	30.00 (±4)	41.72 (± 7.08)	7.30 (± 0.55)	1.76 (± 1.07)	0.19 (± 0.42)	2.82 (± 0.55)	1.69 (± 0.19)
SN1	32.33 (± 1.52)	47.20 (± 8.76)	8.95 (± 0.14)	2.61 (± 0.00)	1.71 (± 0.52)	4.14 (± 0.68)	1.90 (±0.01)
SN2	25 (± 4.35)	38.98 (± 3.91)	10.17 (± 1.25)	3.98 (± 0.46)	1.84 (± 0.00)	3.23 (± 0.63)	1.92 (±0.19)
SN3	24.66 (± 6.80)	28.22 (± 2.71)	6.70 (± 0.97)	1.56 (± 1.27)	0.55 (± 0.23)	3.29 (± 0.45)	2.28 (±0.45)

Table 3. Mean values and standard deviation of xanthophyll epoxidation state (EPS), water potential (Ψ) (Mpa) and stomatal conductance (Gs) ($\text{mmol H}_2\text{O m}^{-2}\text{s}^{-1}$) calculated for each study area for *Pinus sylvestris* and *Pinus nigra*. Measurements obtained at 12:00 GMT.

Study area	EPS	Ψ	Gs
<i>Pinus sylvestris</i>			
SS1 (Not stressed)	0.85±0.08*	-0.53±0.03*	50.91±9.44*
SS2 (Moderate stress)	0.75±0.11*	-0.63±0.02*	43.99±9.04*
SS3 (Stressed)	0.58±0.14*	-0.77±0.06*	36.24±6.44*
*p < 0.05			
<i>Pinus nigra</i>			
SN1 (Not stressed)	0.85±0.05*	-0.40±0.01*	64.86±9.35*
SN2 (Moderate stress)	0.80±0.11*	-0.43±0.01*	57.64±9.62*
SN3 (Stressed)	0.70±0.10*	-0.50±0.01*	44.636±9.84*
*p < 0.05			

Table 4. Photochemical reflectance index formulations and structural vegetation indices used in this study and indices calculated from the AHS bandset.

	Equation	Reference
PRI ₅₇₀	$(R_{570}-R_{531})/(R_{570}+R_{531})$	Gamon <i>et al.</i> (1993)
PRI _{m1}	$(R_{512}-R_{531})/(R_{512}+R_{531})$	This study
PRI _{m2}	$(R_{600}-R_{531})/(R_{600}+R_{531})$	Gamon <i>et al.</i> (1993)
PRI _{m3}	$(R_{670}-R_{531})/(R_{670}+R_{531})$	Gamon <i>et al.</i> (1993)
PRI _{m4}	$(R_{570}-R_{531}-R_{670})/(R_{571}+R_{531}+R_{670})$	This study
NDVI	$(R_{NIR} - R_{red}) / (R_{NIR} + R_{red})$	Rouse <i>et al.</i> (1974)
SR	(R_{NIR}/R_{red})	Jordan (1969); Rouse <i>et al.</i> (1974)
OSAVI	$(1 + 0.16) * (R_{800} - R_{670}) / (R_{800} + R_{670} + 0.16)$	Rondeaux <i>et al.</i> (1996)
MSAVI	$\frac{1}{2} \left[2 * R_{800} + 1 - \sqrt{(2 * R_{800} + 1)^2 - 8 * (R_{800} - R_{670})} \right]$	Qi <i>et al.</i> (1994)
MTVI ₂	$\frac{1.5 * [1.2 * (R_{800} - R_{550}) - 2.5 * (R_{670} - R_{550})]}{\sqrt{(2 * R_{800} + 1)^2 - (6 * R_{800} - 5 * \sqrt{R_{670}}) - 0.5}}$	Haboudane <i>et al.</i> (2004)

Table 5. Nominal values and range of parameters used for leaf and canopy modeling with LIBERTY and INFORM for *Pinus nigra*.

<i>Leaf optical and structural parameters</i>	Units	Values
Hemispherical reflectance and transmittance of green leaves	nm	Measured
Average internal cell diameter (D)	μm	65
Intercellular Air Space Determinant (<i>xu</i>)	/	0.06
NeedleThickness	/	4.09
Linear (Baseline) Absorption	/	0.0006
Albino Leaf Absorption	/	1.25
Leaf Chl a+b content	mg/m^2	100 - 500
Leaf Equivalent Water	g/m^2	100
Lignin / Cellulose Content	g/m^2	40
Protein Content	g/m^2	1
<i>Canopy structural parameters</i>		
LAI	m^2/m^2	1 - 3
n° trees/ha	/	800 - 2800
Crown height	m	7.9
Crown diameter	m	3.7
<i>Background and viewing geometry</i>		
Solar zenith and azimuth	Degrees	190.68
Instrument solar zenith and azimuth	Degrees	17.7
Soil reflectance	mm	Measured

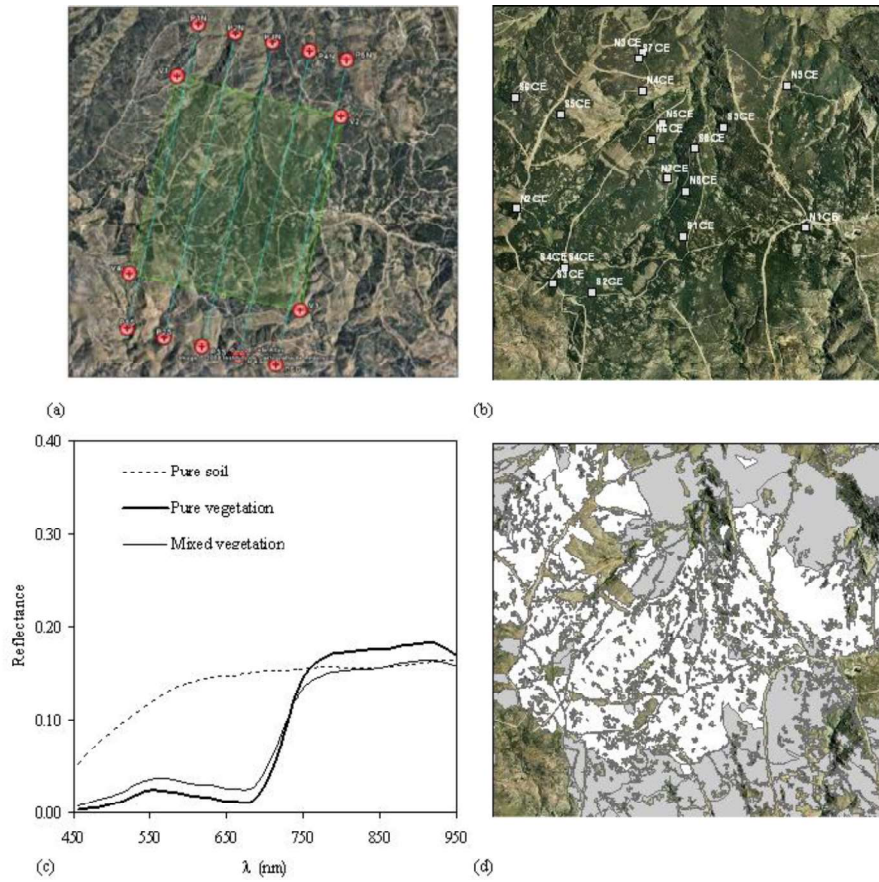


Figure 1. AHS airborne footprint (a). Overview of the area acquired with the AHS instrument (b). Single pixel AHS spectra for pure vegetation, soil and mixed vegetation-soil pixels (c). Distribution of *Pinus sylvestris* (white) and *Pinus nigra* (grey) on the study area (d).

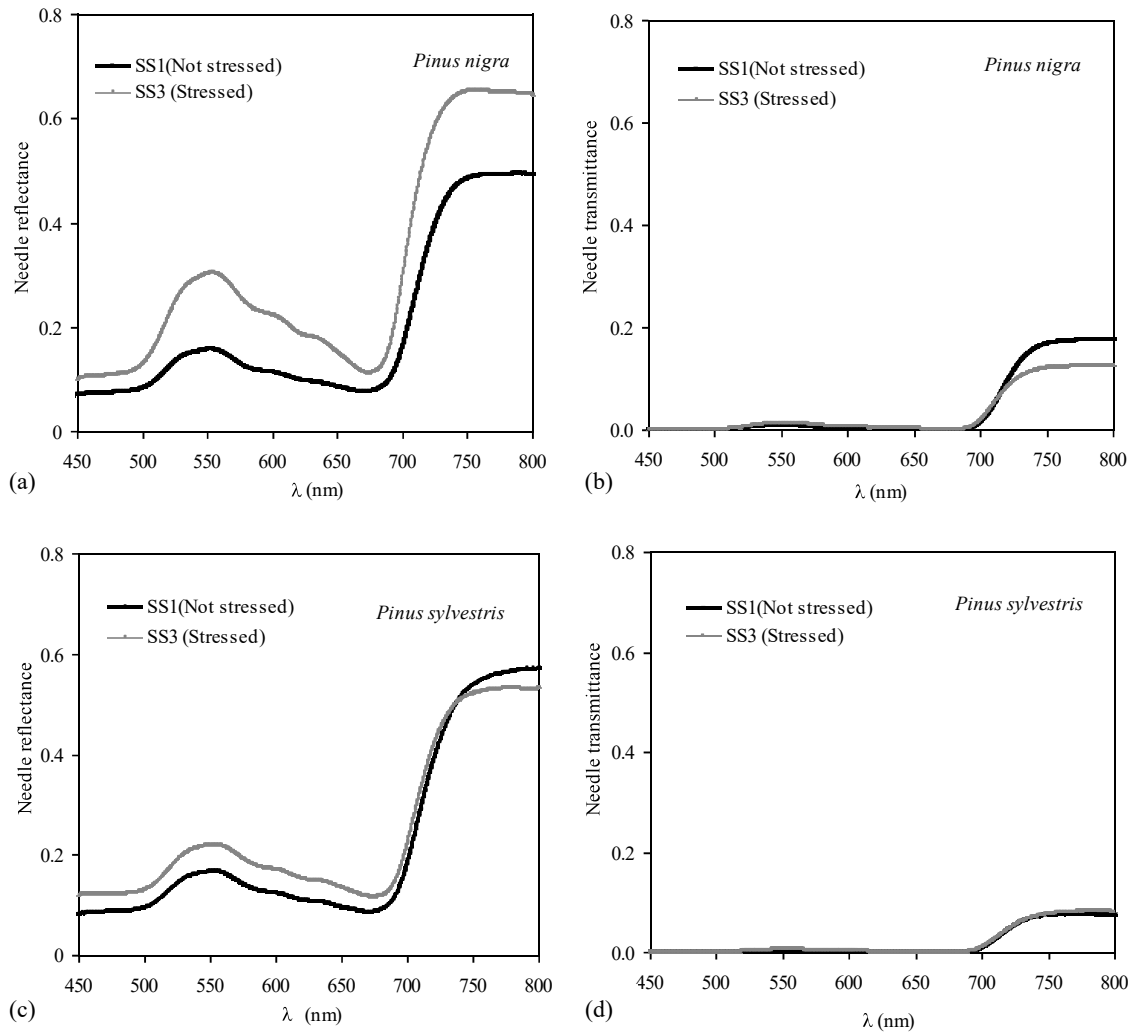
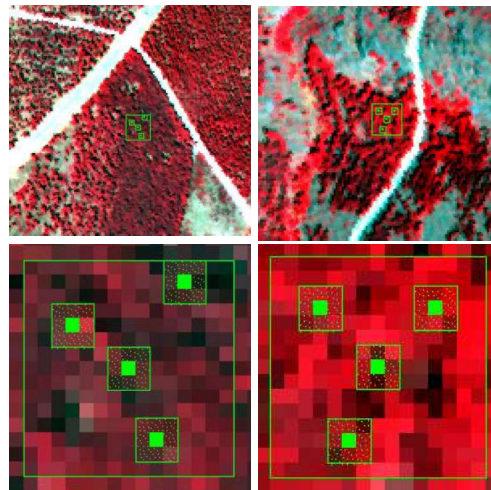
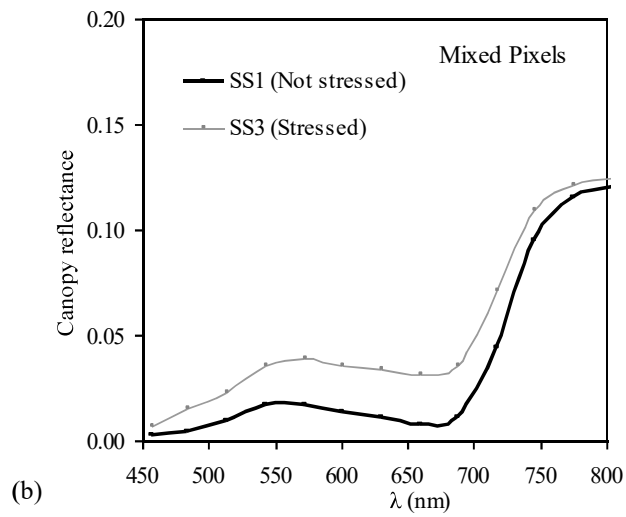
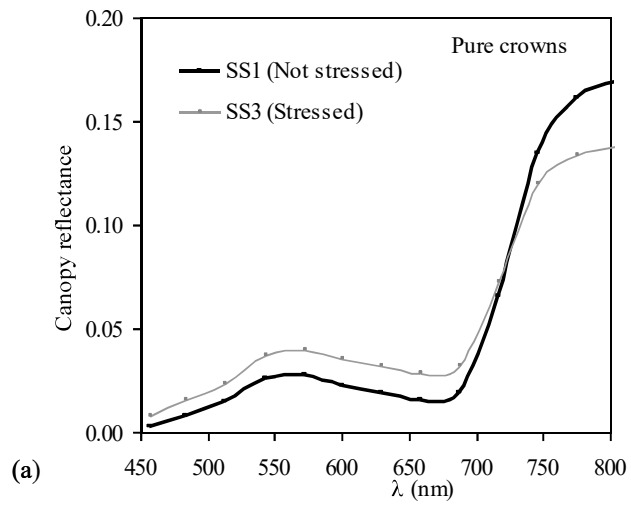


Figure 2. Needle reflectance and transmittance measurements collected with a Li-Cor 1800-12 integrating sphere corresponding to *Pinus nigra* (a, b) and *Pinus sylvestris* (c, d) from stressed and non-stressed study areas.



(c)

Figure 3. AHS spectra for *Pinus sylvestris* of (a) pure tree crowns and (b) mixed pixels comprising pure crown, soil and shadow. (c) Example of stressed and non-stressed study areas for *Pinus sylvestris*.

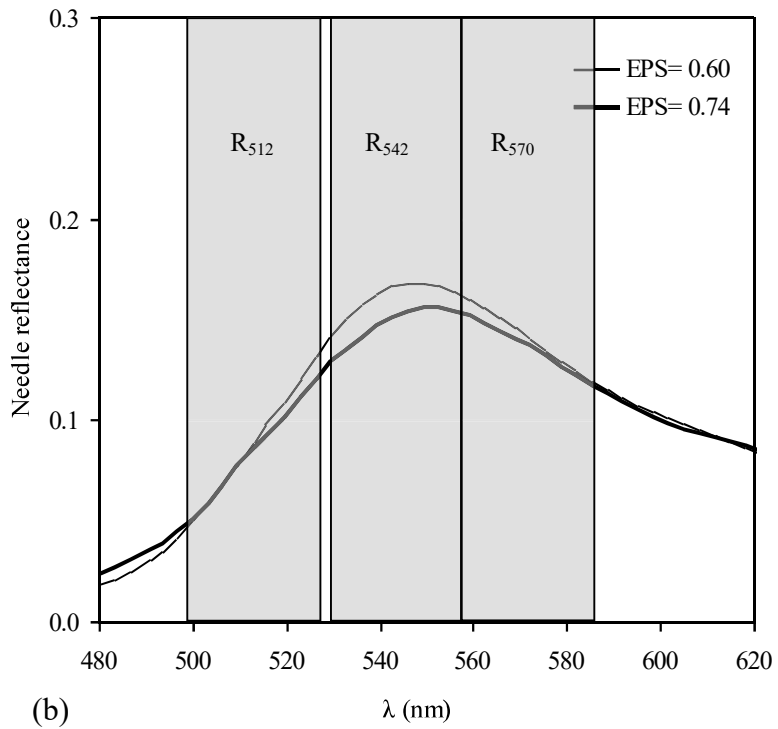
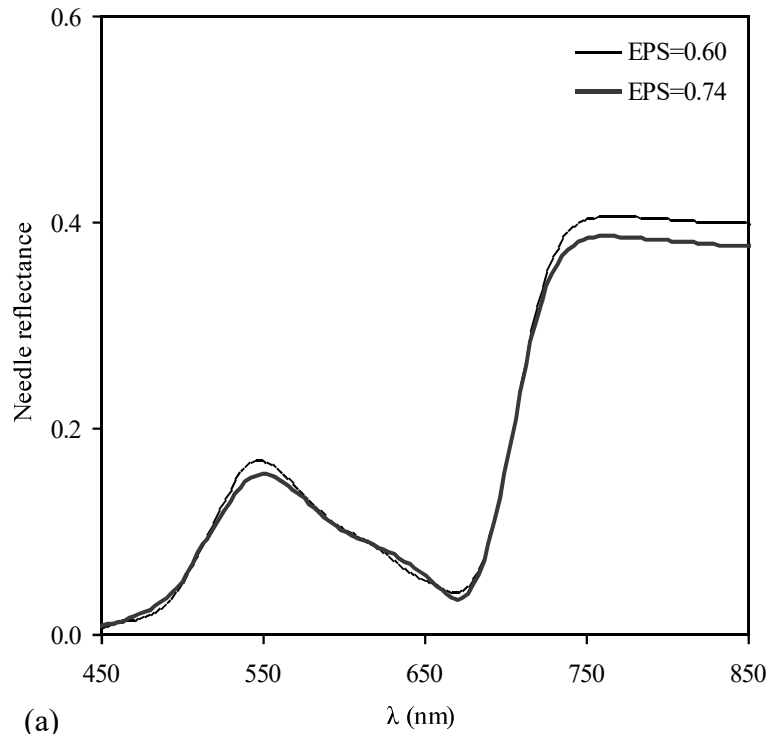


Figure 4. (a) Spectral reflectance of needles of *Pinus sylvestris* with different epoxidation state of the xanthophylls (EPS) values. (b) Zoom of the region of absorption of the xanthophylls cycle and center wavelength and bandwidth for the AHS bands used to calculate PRI (R_{512} , R_{542} , R_{571}). Measurements obtained at 12:00 GMT.

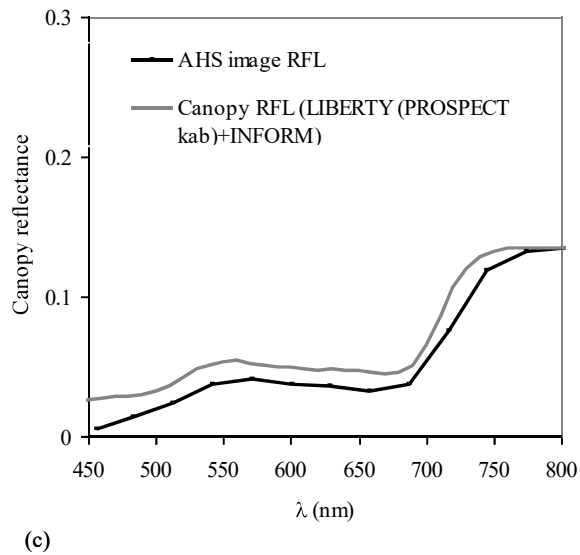
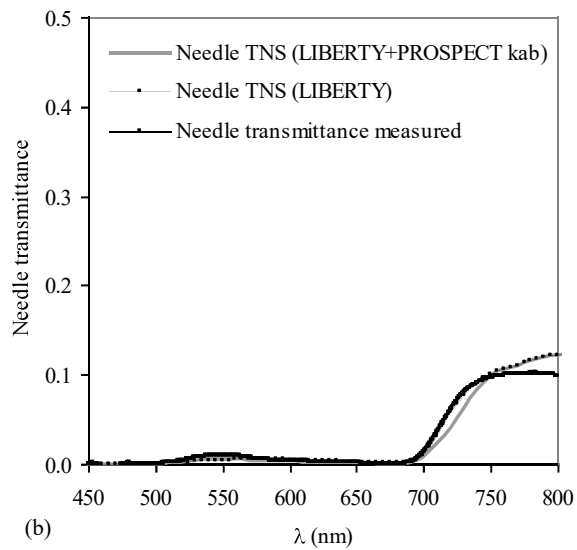
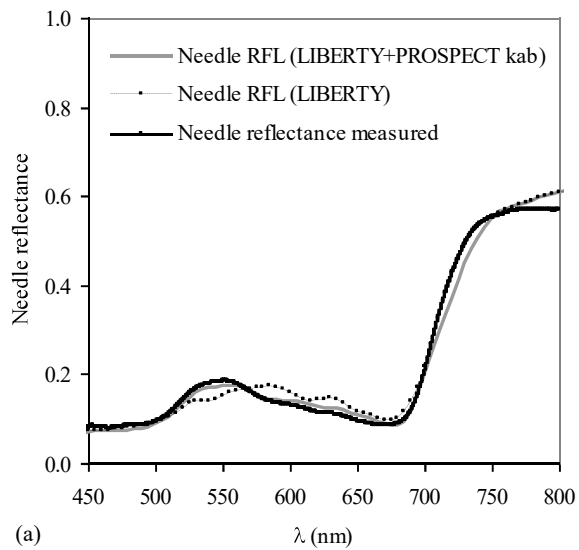


Figure 5. Needle reflectance (RFL) (a) and transmittance (TNS) (b) measured with the integrating sphere, simulated with LIBERTY and simulated with LIBERTY using the absorption coefficient of PROSPECT. Crown reflectance spectra obtained from the AHS image and simulated with LIBERTY+INFORM (c).

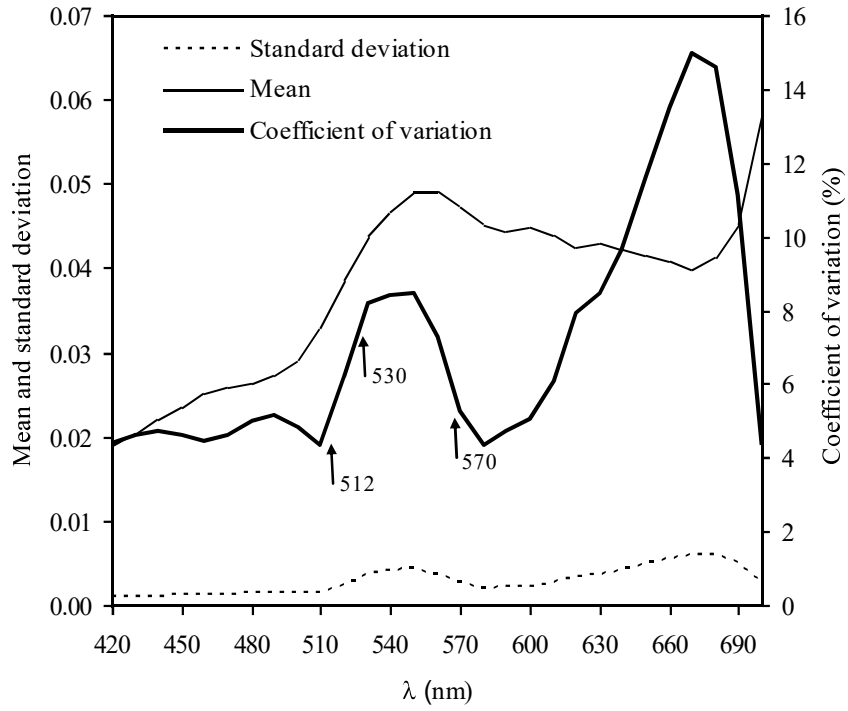


Figure 6. Mean, coefficient of variation (CV), and standard deviation of spectral reflectance for LAI ranges (1-3) and tree densities (800-2800 trees/ha) simulated with the coupled LIBERTY+INFORM model.

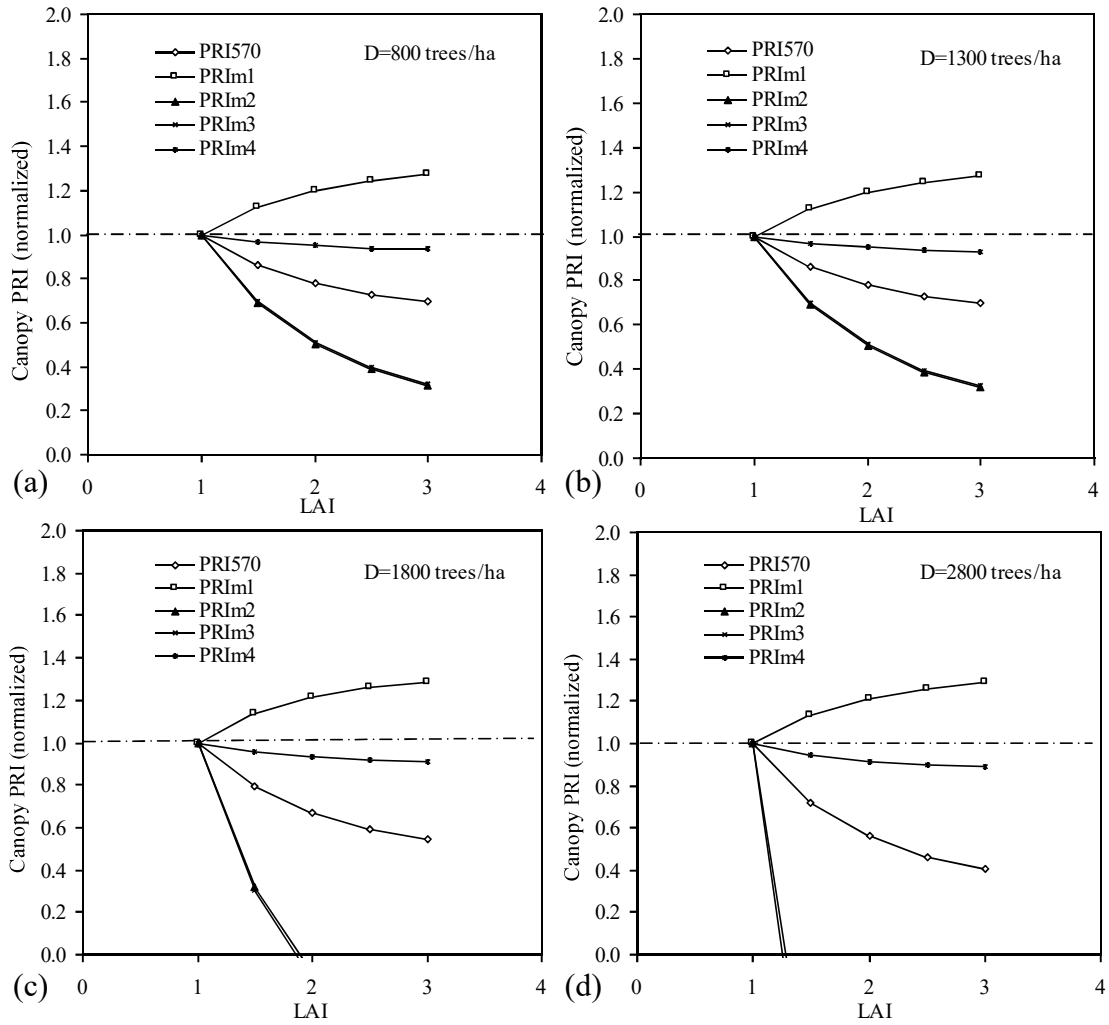


Figure 7. Model simulations conducted with INFORM for PRI₅₇₀ and modified PRI formulations. Results obtained by simulating the plot reflectance with different densities (D) and LAI values. Results normalized for LAI=1. Tree densities (D) used were a) 800, b) 1300, c) 1800, d) 2800 trees/ha.

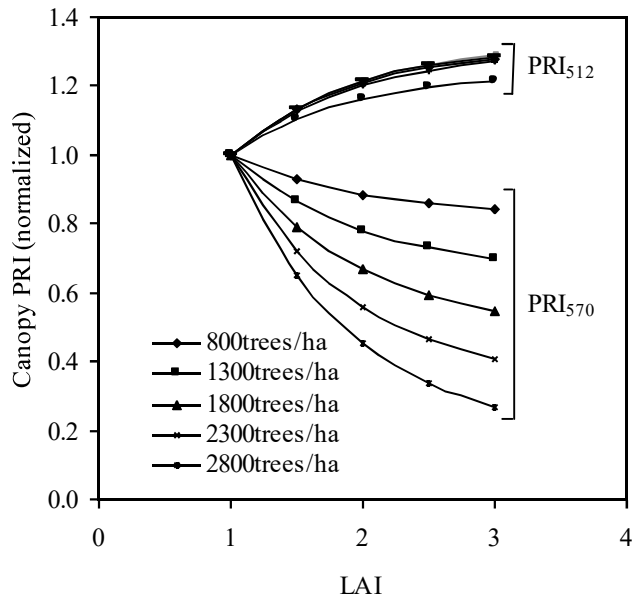


Figure 8. Model simulations conducted with INFORM for PRI₅₇₀ and PRI₅₁₂. Results obtained by simulating the plot reflectance with different densities (D) and LAI values. Results normalized to LAI=1.

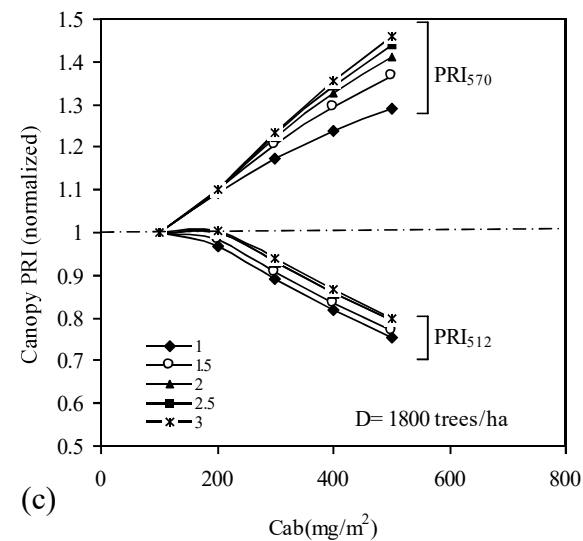
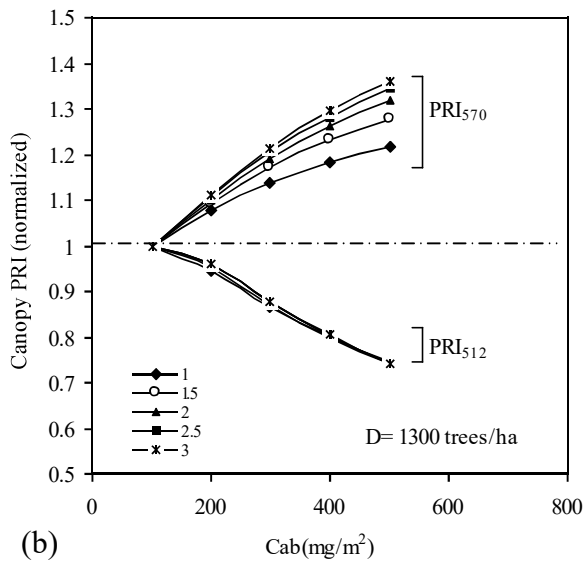
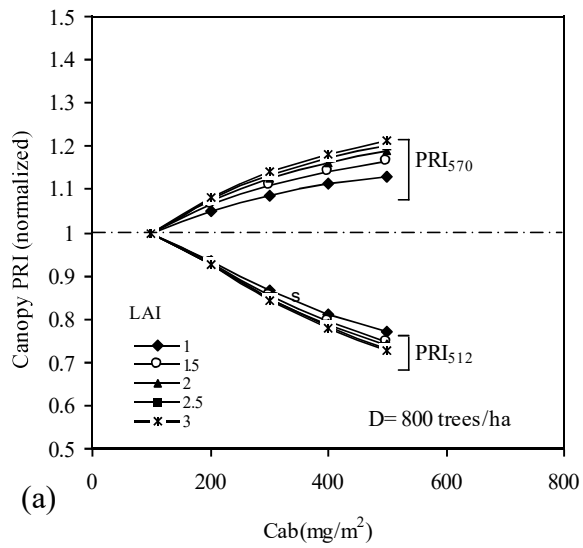


Figure 9. Model simulations conducted with INFORM for canopy PRI_{570} and PRI_{512} for different values of chlorophyll (Cab). Results obtained by simulating the plot reflectance with different values of LAI for a) 800 trees/ha, b) 1300 trees/ha, c) 1800 trees/ha.

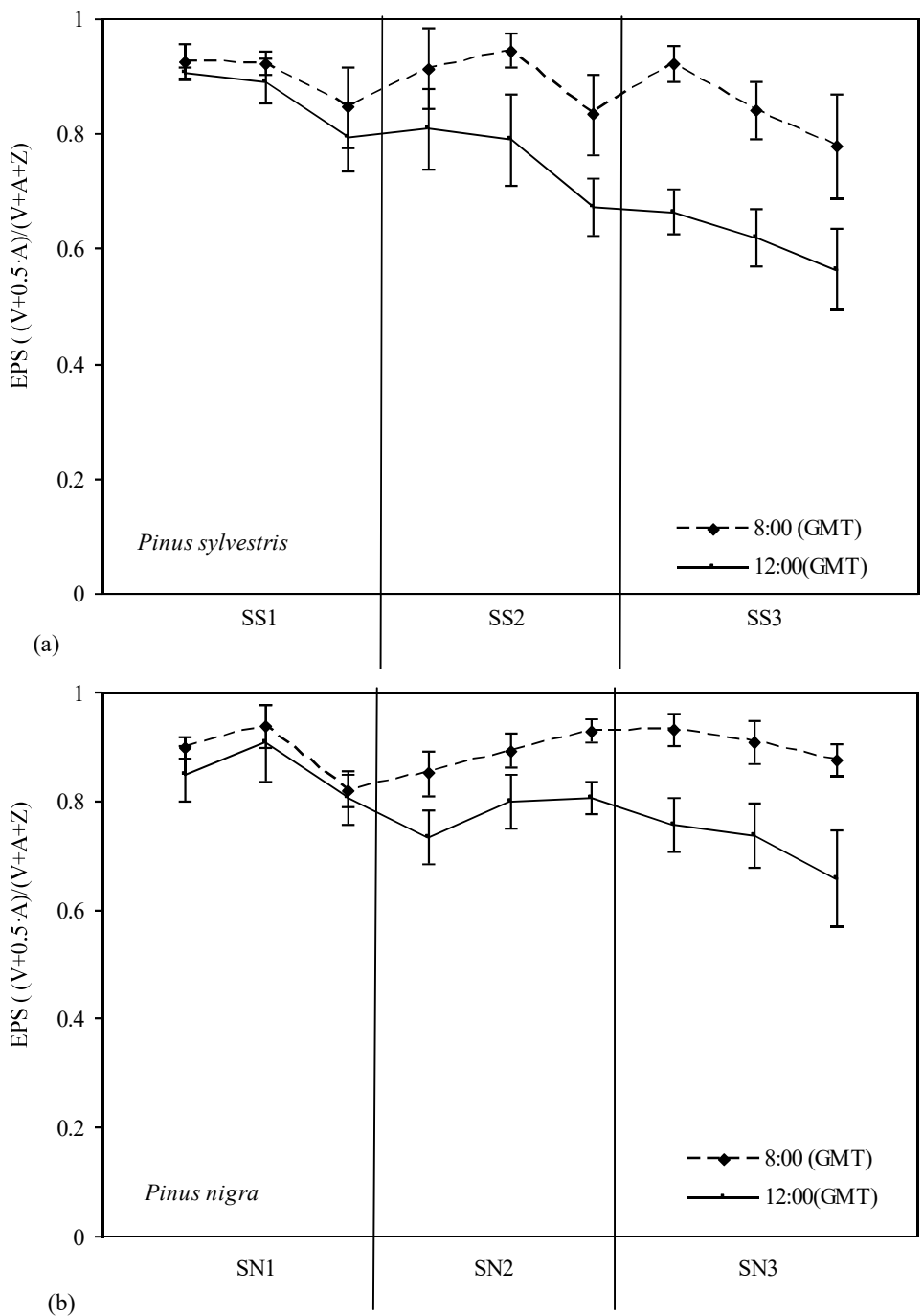


Figure 10. Comparison between the epoxidation state of the xanthophylls pigments at 8:00 and 12:00 GMT measured at each study areas (SS1, SS2, SS3) for *Pinus sylvestris* (a) and (SN1, SN2, SN3) for *Pinus nigra* (b). The value on each plot is the mean EPS of the four trees measured per plot and the corresponding standard deviation.

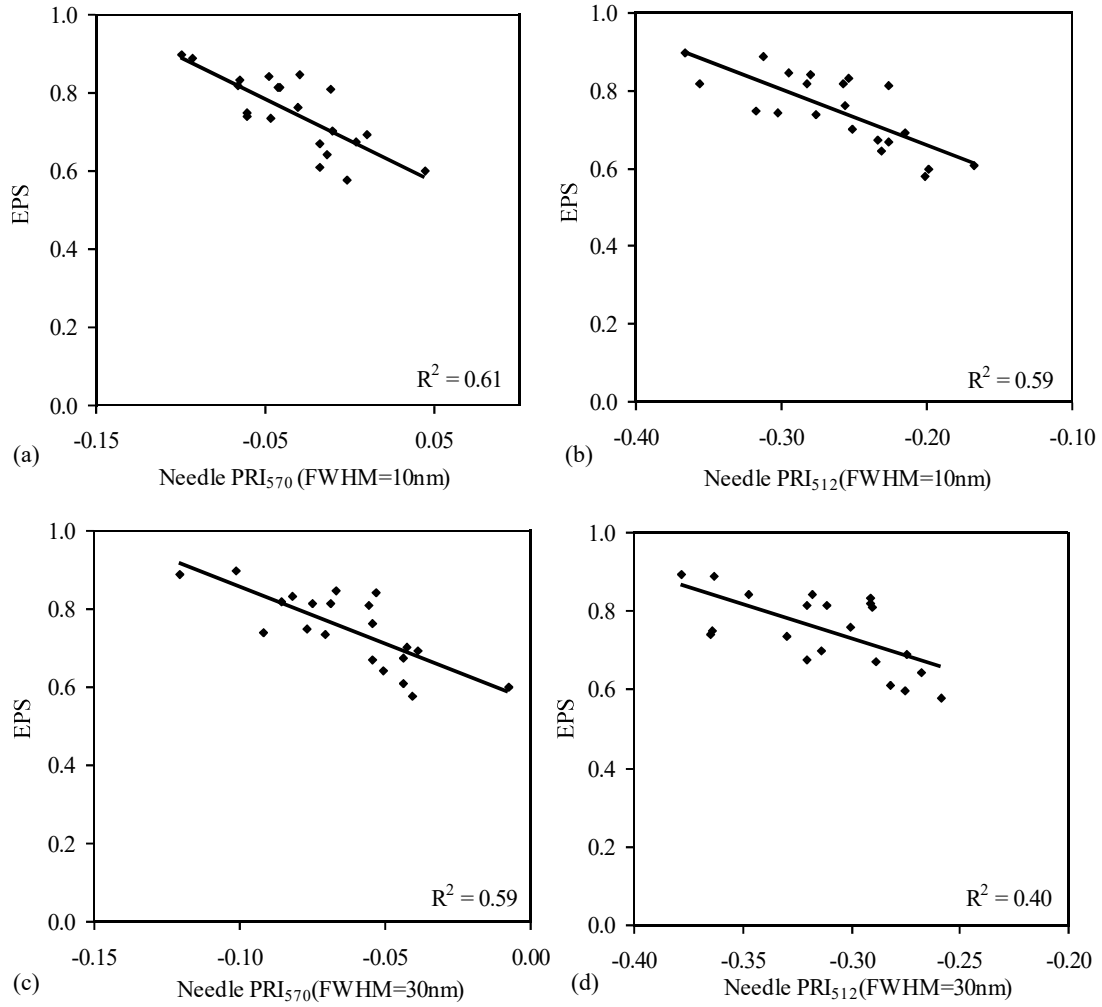


Figure 11. Relationships obtained between the epoxidation state of the xanthophylls pigments $EPS = (V + 0.5 \cdot A) / (V + A + Z)$ and PRI₅₇₀ for FWHM of 10nm (a) and 30nm (c), and PRI₅₁₂ with FWHM of 10nm (b) and 30nm (d). Needle measurements obtained at 12:00 GMT from crowns with different levels of stress on *Pinus sylvestris*.

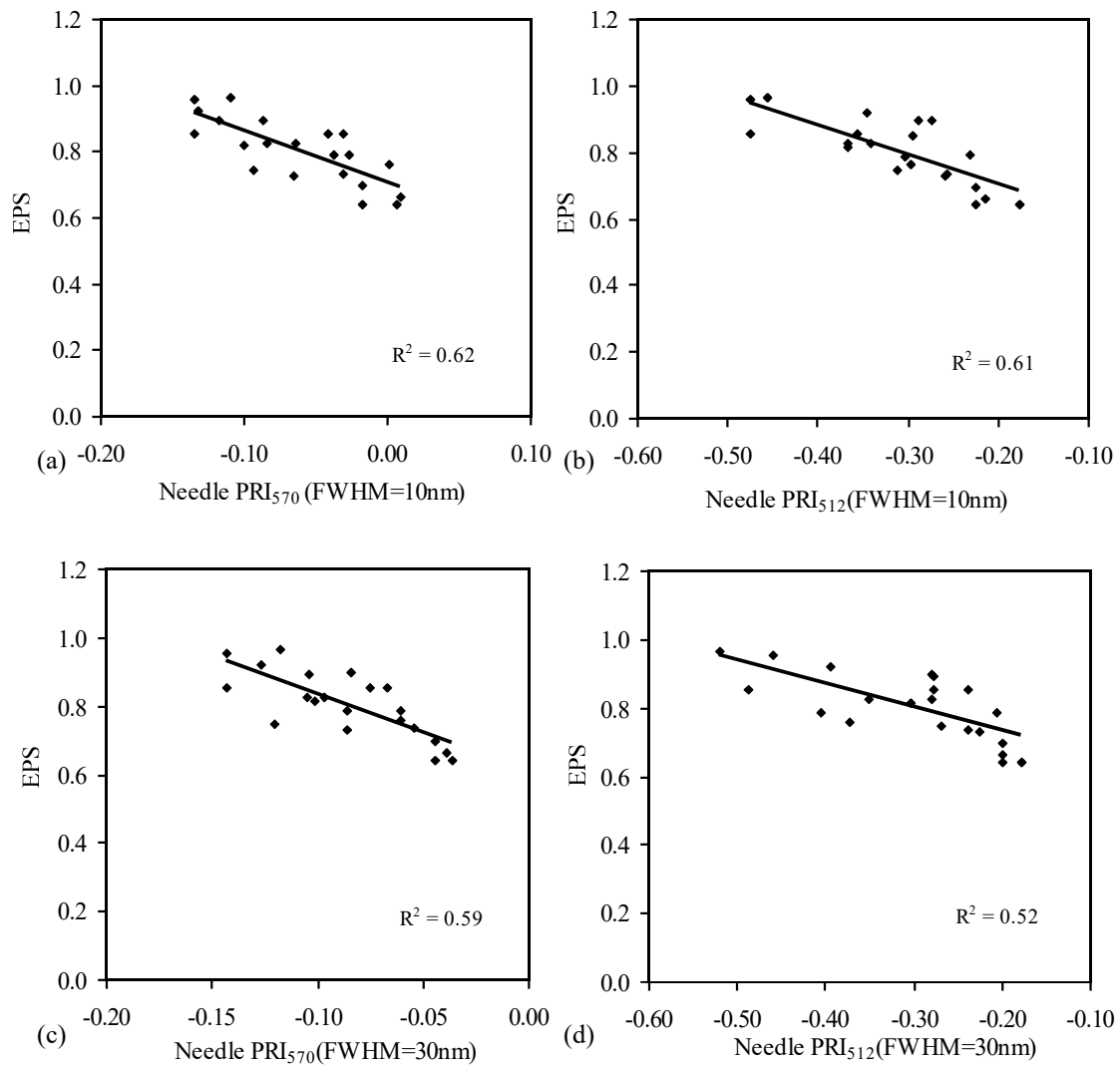


Figure 12. Relationships obtained between the epoxidation state of the xanthophylls pigments $EPS = (V + 0.5 \cdot A) / (V + A + Z)$ and PRI_{570} for FWHM of 10nm (a) and 30nm (c), and PRI_{512} with FWHM of 10nm (b) and 30nm (d). Needle measurements obtained at 12:00 GMT from crowns with different levels of stress on *Pinus nigra*.

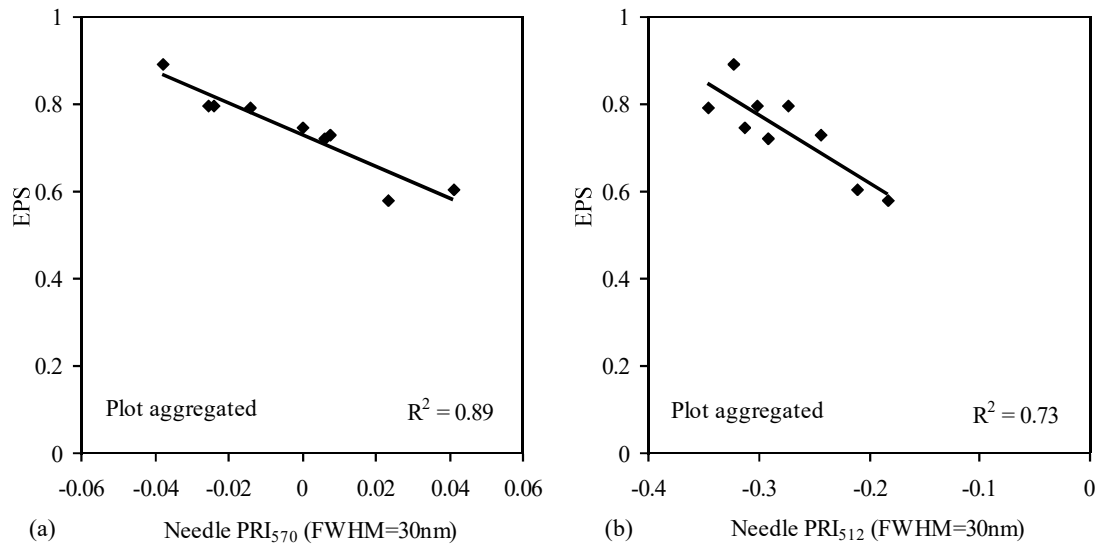


Figure 13. Leaf-level relationships obtained between the epoxidation state of the xanthophylls pigments $EPS = (V + 0.5 \cdot A) / (V + A + Z)$ and PRI₅₇₀ (a) and PRI₅₁₂ (b) both with FWHM of 30nm. Needle measurements obtained at 12:00 GMT at the plot level with different levels of stress on *Pinus sylvestris*.

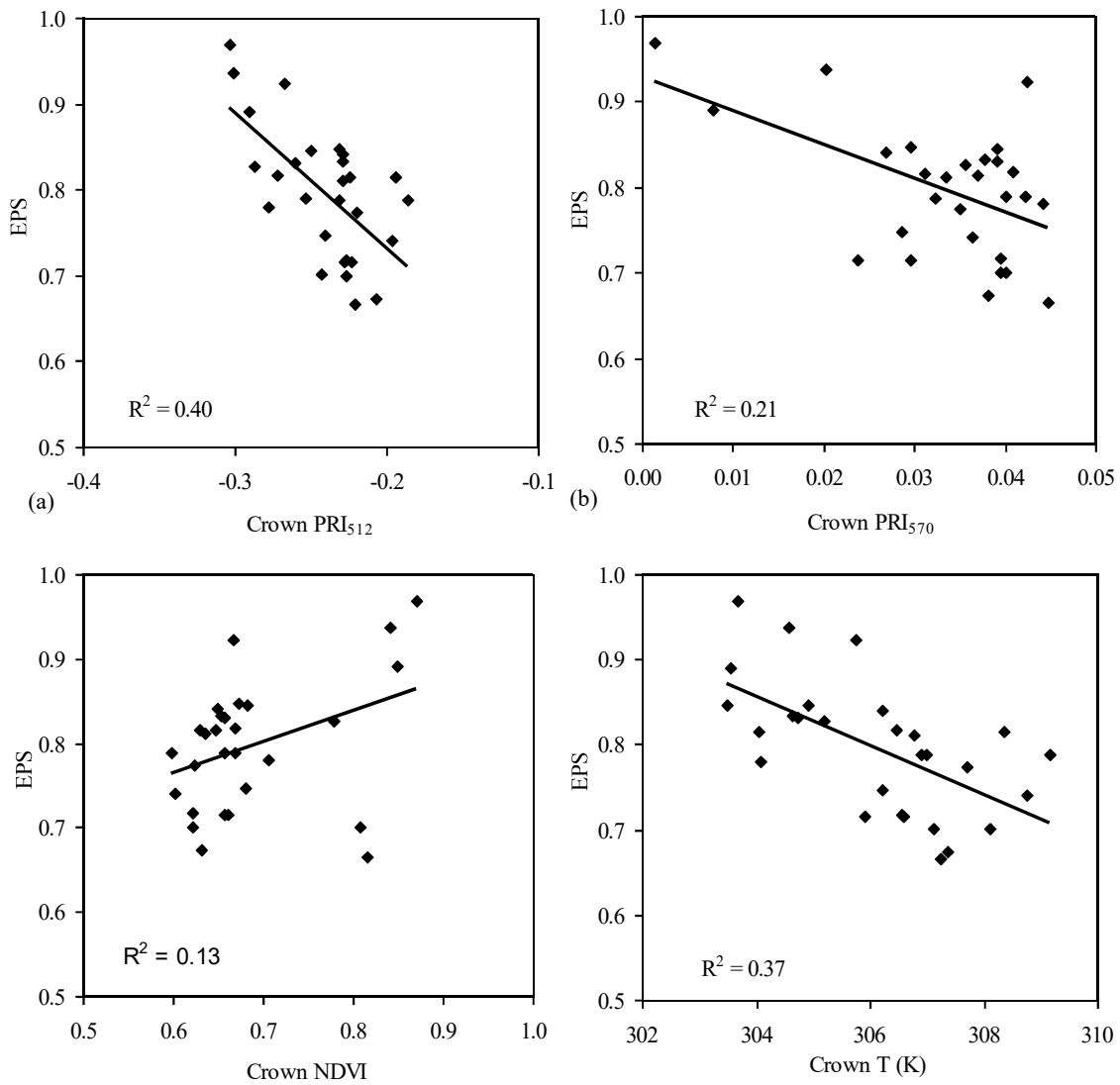


Figure 14. Crown-level relationships obtained between the epoxidation state of the xanthophylls $EPS = (V+0.5*A)/(V+A+Z)$ and vegetation indices: NDVI (a), PRI₅₇₀ (b) and PRI₅₁₂ (c). Needle measurements obtained at 12:00 GMT from crowns with different levels of stress on *Pinus sylvestris* and NDVI > 0.6. PRI₅₇₀, PRI₅₁₂ and T obtained from the AHS airborne sensor.

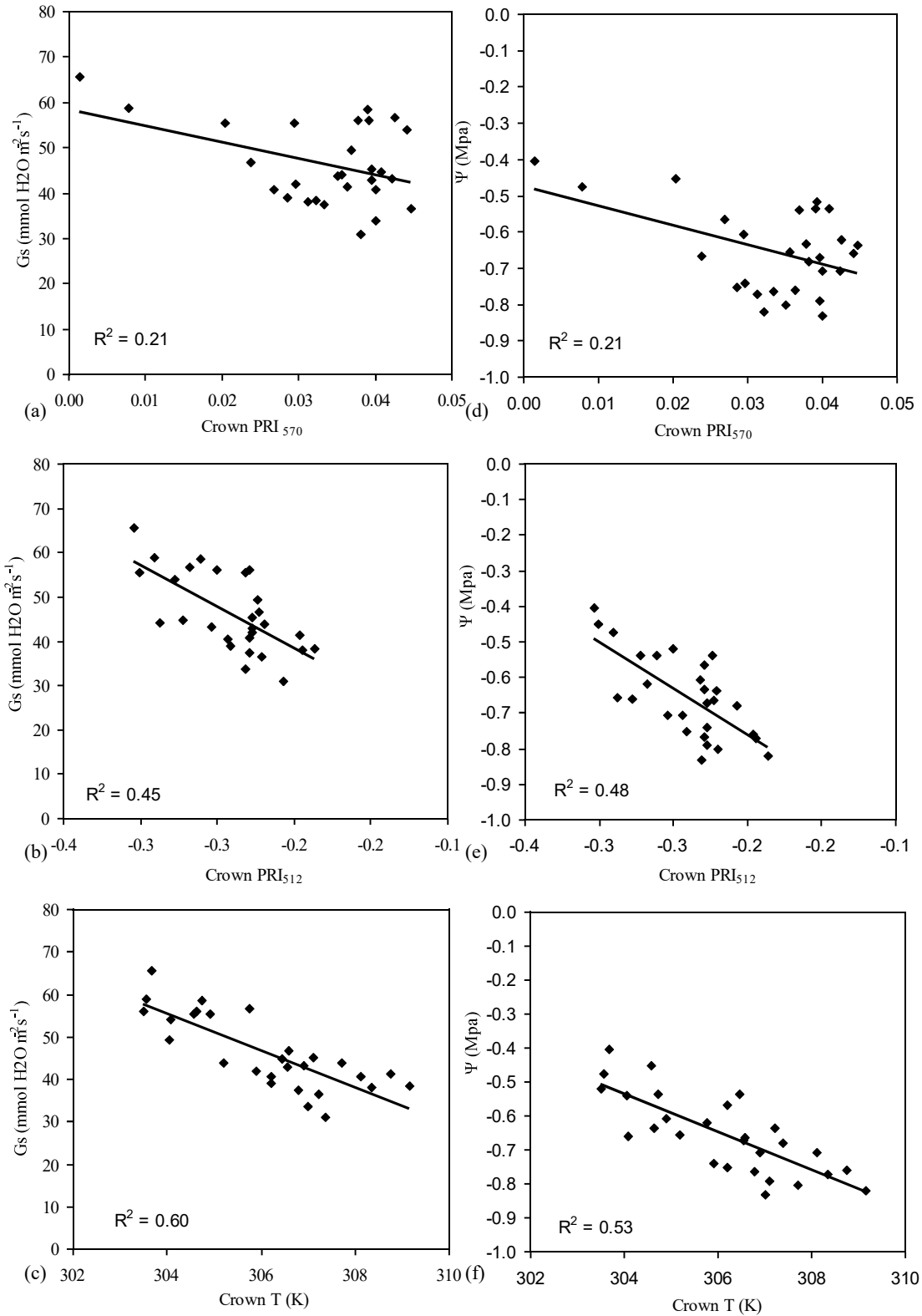


Figure 15. Crown-level relationships obtained for *Pinus sylvestris* between the stomatal conductance (G_s) and PRI_{570} (a), PRI_{512} (b) and temperature (T) (c). Crown-level relationships between midday water potential (Ψ) and PRI_{570} (d), PRI_{512} (e) and temperature (T) (f) of trees with $\text{NDVI} > 0.6$.

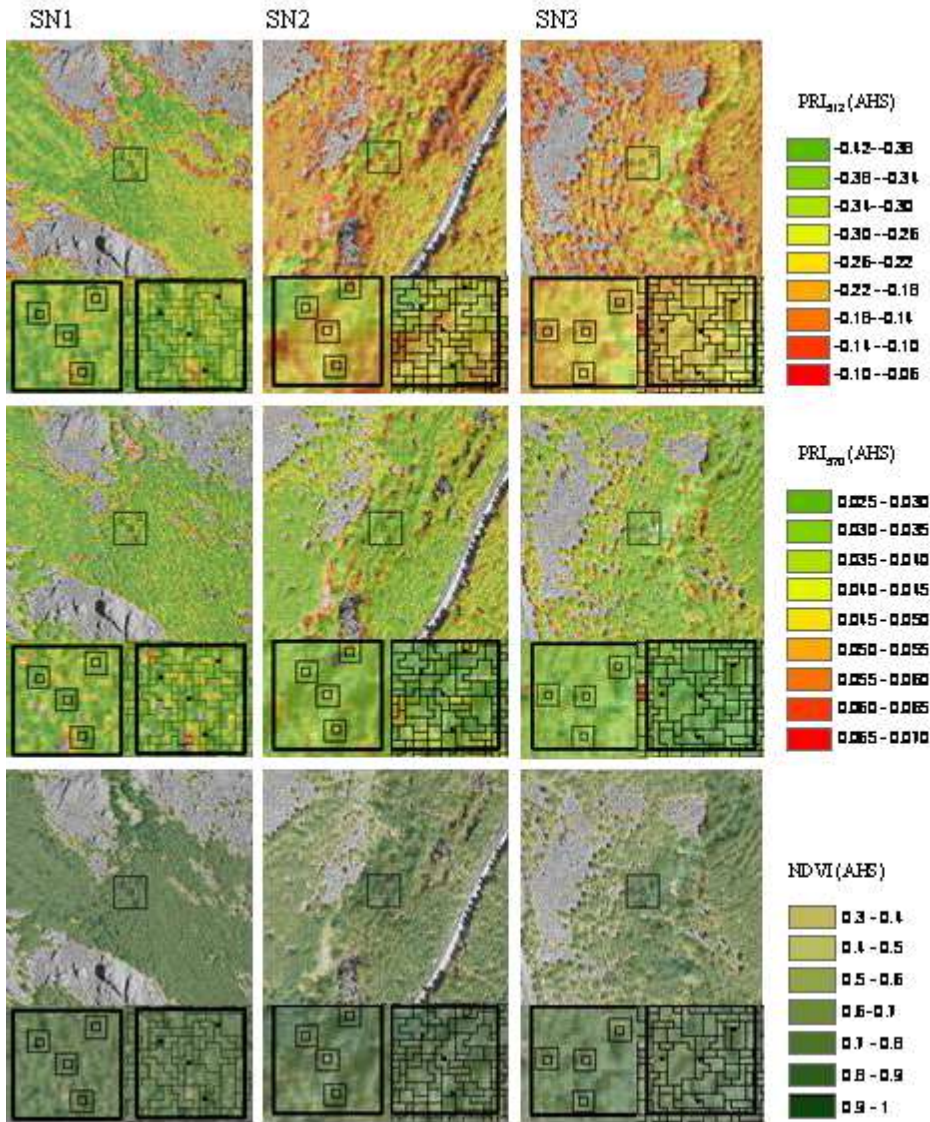


Figure 16. PRI_{512} , PRI_{570} and NDVI obtained from the AHS airborne sensor from three study areas of *Pinus nigra* with different levels of stress: SN1, SN2 and SN3. At the bottom of each image, two zoom images of a central plot, one pixel-based displaying 1x1 and 3x3 resolutions and the other at object level.

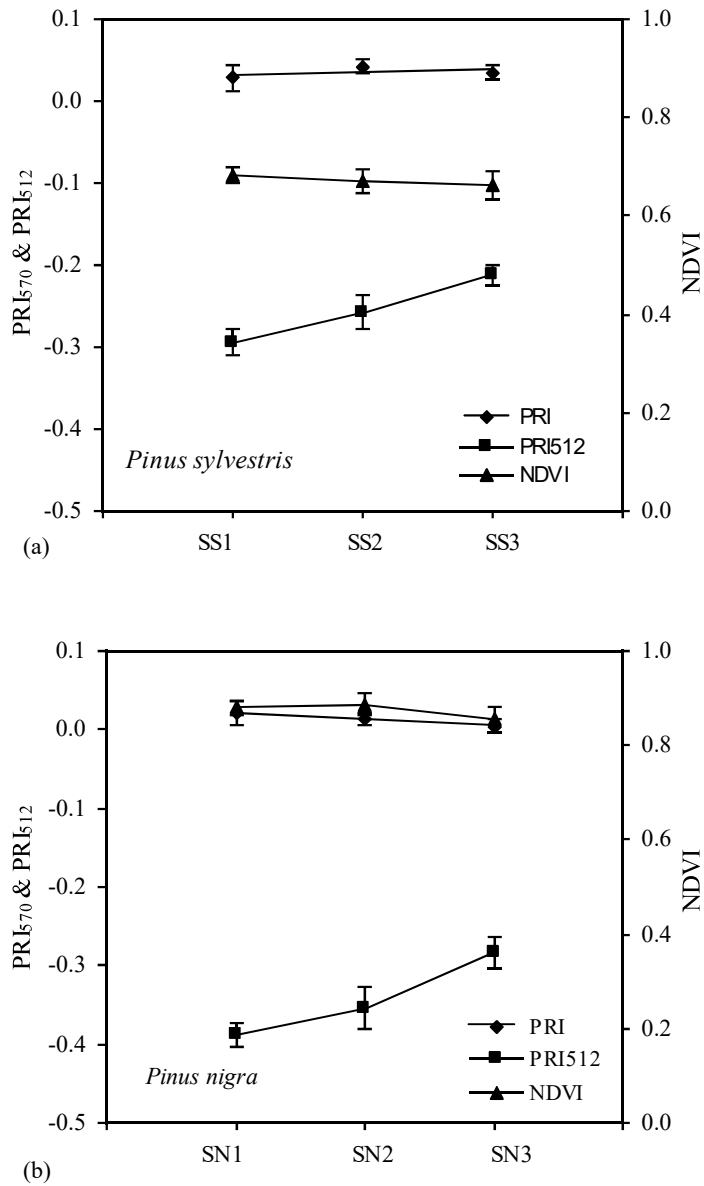


Figure 17. Mean values and standard deviation obtained from the AHS image of PRI₅₇₀, PRI₅₁₂ and NDVI. Values calculated from twelve trees located in the study areas SN1, SN2 and SN3 of *Pinus nigra* (a) and SS1, SS2 and SS3 of *Pinus sylvestris* (b).